The space-time architecture variation of the shallow magmatic plumbing systems feeding the Campi Flegrei and Ischia volcanoes (Southern Italy) from halogen constraints

Manuscript 8883 R2

Balcone-Boissard Hélène[1], Boudon Georges[2], Zdanowicz Géraldine[1,2], Orsi Giovanni[3], Webster Jim [4], Civetta, Lucia[3], D'Antonio, Massimo[3], Arienzo Ilenia[5]

Author names and affiliations

[1] *ISTeP - Sorbonne Université, CNRS, 4 place Jussieu 75005 Paris, France*

[2] *Université de Paris, Institut de physique du globe de Paris, CNRS, F-75005 Paris, France*

[3] *Dipartimento di Scienze della Terra, dell'Ambiente e delle Risorse, Università degli Studi di Napoli Federico II, Via Vicinale Cupa Cintia 21, 80126 Napoli, Italy*

[4]*Department of Earth and Planetary Sciences, American Museum of Natural History, Central Park West at 79th St., NY, NY 10024-5192 USA*

[5]*Istituto Nazionale di Geofisica e Vulcanologia, Sezione Osservatorio Vesuviano, Via Diocleziano 328, 80124 Napoli, Italy*

Corresponding author

Balcone-Boissard Hélène: helene.balcone_boissard@sorbonne-universite.fr

Abstract

For active volcanoes, knowledge of the architecture of the plumbing system and the conditions of magma storage prior to an eruption are highly important given their influence on the eruptive style and thus the management of future volcanic crises. Here chlorine is used as a geobarometer for potassic alkaline magmas at the Campi Flegrei volcanic complex, revealing the shallowest depth of fluid-melt equilibration with respect to Cl. The results for representative fallout deposits of selected explosive eruptions show the existence of a multi-depth equilibration zone through time, including shallow magma storage. We describe evidence for the shallowest zone located at a depth equivalent to 65 MPa for the Agnano Monte Spina eruption (4,482–4,625 cal. yrs BP), at ~100 MPa for the Pomici Principali (11,915–12,158 cal. yrs BP) and the Astroni 6 (4,098–4,297 cal. yrs BP) eruptions, and close to 115 MPa for the last explosive eruption of Monte Nuovo (AD 1538). For comparison, the pressure estimated for a possible reservoir feeding the Cretaio eruption of Ischia island (AD 430), the only studied eruption on Ischia, is ~140 MPa. The pressure estimates for the two largest magnitude eruptions, the Campanian Ignimbrite (39 ka) and the Neapolitan Yellow Tuff (14.9 ka), are also discussed with respect to available magma withdrawal models. The pressures estimated using the Cl geobarometer for the magma leading to the fallout phases of these two eruptions provide evidence for a low-volume shallow domain (~40 MPa) for the Plinian phase of the Campanian Ignimbrite eruption and a main, deeper reservoir (~130–165 MPa) for the Neapolitan Yellow Tuff eruption. The inferred shallowest equilibration pressures are interpreted here as corresponding to transitory, short-lived magma apophyses whose eruption may have been facilitated by optimum tectonic stresses, rheological behavior of the crust and efficiency of volatile exsolution. Alternatively, these magma apophyses may represent an evolved, crystal-rich ponded magma into which a volatile-rich magma ascending from depth was injected. The transient nature of such very shallow reservoirs is suggested by the short timescales inferred from diffusion modelling on crystals available in the literature for the studied Campi Flegrei eruptions.

The influence of sulfur (S) on Cl solubility is assessed through Cl solubility modelling and applied to different eruptions. In addition, the pressure at which magmatic fluids and melts equilibrated with respect to Cl is shallower for the Campi Flegrei volcanic complex than the Somma-Vesuvio volcanic complex, erupting more homogeneous differentiated magma, of trachytic or phonolitic composition. This approach of using Cl to investigate the architecture of the plumbing system can be extended to all alkali-rich magma systems.

Highlights

- H1: Cl acts as a geobarometer for alkaline magmas emitted at Campi Flegrei and Ischia
- H2: contrasted architecture and dynamics of magma plumbing system of ignimbritic eruptions compared to other eruptions
- H3: the H-C-O-S-Cl-F system has to be considered when discussing volatile behavior

Keywords

Campi Flegrei, Ischia, Chlorine, geobarometer, alkaline magmas, pre-eruptive conditions

DOI: https://doi.org/10.2138/am-2022-8883. http://www.minsocam.org/

1. Introduction

The chemical and physical characteristics of erupted magmas result from a combination of processes occurring at depth in the crust, during both magma storage and ascent. The shallow crustal reservoirs of a given magmatic system are thus key environments as their characteristics constrain both the composition of the extruded magma and the style of the eruption (Bower and Woods, 1998; Andujar et Scaillet, 2012; Bachmann and Huber, 2016; Popa et al., 2019). Therefore, establishing their location, as well as the pre-eruptive magma conditions, both chemical (e.g., composition, amount of volatiles, fluid saturation condition) and physical (e.g., viscosity, density), is of primary importance (Goepfert and Gardner, 2010; Parmigiani et al., 2017; Edmonds and Woods, 2018; Huber et al., 2019; Popa et al., 2021a, b;)

The general concept of the dynamic architecture of the magma plumbing system has undergone revision recently (Cashman et al., 2017; Bachmann and Huber, 2016: Magee et al., 2018). The crustal plumbing system results from the degree of connection between multi-depth transient batches of magma of variable composition. Their location, shape and magma storage conditions can be assessed by different means. Geophysical surveys (mostly seismic reflection) provide useful information on the location and shape of existing reservoirs (Pritchard and Gregg, 2016 and references therein). The petrology of volcanic products provides a valuable tool for defining pre-eruptive conditions of the magmatic reservoirs feeding past and ongoing events (Blundy and Cashman, 2008; Samaniego et al., 2011; Gurioli et al., 2017; Berthod et al., 2021; Re, 2021; Pontesilli et al., 2023). This includes melt inclusion (MI) chemistry (e.g., Wallace, 2005) and mineral-melt thermobarometry, which provides constraints on the depth at which magmas formed, stagnated and/or equilibrated in the lithosphere (e.g., Putirka, 2008, and references therein).

This is the peer-reviewed, final accepted version for American Mineralogist, published by the Mineralogical Society of America.
The published version is subject to change. Cite as Authors (Year) Title. American Mineralogist, in press.
DOI: https://doi.org/10.2138/am-2022-8883. http://www.minsocam.org/

Experimental petrology also provides strong constraints on the prevailing conditions at depth, using laboratory experiments to reproduce the P, T, fO_2, and P_{H2O} conditions that prevailed during crystallization of the phase assemblage of the erupted products (e.g., Scaillet et al., 2008).

This article presents and discusses the results of a study based on the application of the Cl geobarometer, and is aimed at improving current understanding on the evolution of the magmatic systems feeding the volcanoes of the Phlegraean Volcanic District (PVD) in the Neapolitan area of southern Italy (Orsi et al., 1996a). The collected data are also compared with those available for the Somma-Vesuvio volcanic complex (SVVC) (Balcone-Boissard et al., 2016).

2. Geological context and volcanological background

The PVD is located in the Campanian volcanic area and includes the Campi Flegrei (CF), Ischia and Procida volcanic fields. Of these three volcanic fields, CF and Ischia are still active and both are dominated by a resurgent caldera (Orsi et al., 1996a, 2022; Santacroce et al., 2003; Orsi, 2022; Orsi et al., 2022; Fig. 1 and SM1 in Supplementary Material). The PVD is located to the west of the SVVC, which is the third most active Neapolitan volcano (Fig. 1b). This volcanic district is inhabited by more than 1.5 million people, making it one of the highest risk volcanic areas on Earth (e.g., Lirer et al. 2010; Orsi et al., 2003; Bevilacqua et al., 2022; and references therein). Volcanism began here prior to 150 ka, and has continued with several explosive, sometimes high-magnitude caldera-forming eruptions, until historical times (Orsi et al., 1996a, 2003; Santacroce et al., 2003; Orsi, 2022, Orsi et al., 2022). Over the last few decades, the CF caldera has experienced several unrest episodes, also known as bradyseismic crises, with significant ground uplift and subsidence, seismicity, gravity changes and variations in geochemical parameters of gas and water effluents. De Siena et al. (2010) suggested that a shallow magma batch was intruded to a depth of about 4 km during the 1982-84 unrest episode. The last and still ongoing of these unrests began in late 2004/early 2005 (Del Gaudio et al., 2010; Ricco et al., 2019; Chiodini et al., 2015, 2022; Scarpa et al., 2022, and references therein). There are various interpretations for the source of these more recent unrest episodes (a comprehensive review can be found in Bonafede et al., 2022). One interpretation of the 2012-2013 episode by D'Auria et al. (2015)involves the intrusion of ~0.004 km^3 of magma at shallow depth (~3 km). The authors believe that these results can be extrapolated to other events that have occurred over the last 60 years, probably reflecting a persistent shallow magma plumbing structure that has been repeatedly refilled.

The PVD volcanism has been related to extensional processes affecting the Tyrrhenian margin of the Southern Apennines since the Miocene, mainly through NW-SE normal and subordinate NE-SW transverse faults (Moretti et al., 2013b and references therein). The CF, Procida and Ischia volcanoes are NE-SW aligned. The CF and Ischia calderas developed at the intersection of the two major regional fault systems where there is a dense, complex network of tectonic and volcano-tectonic features. This structural setting has generated a localized zone of particularly high permeability within the lithosphere, allowing ascent and deep-to-shallow emplacement of volatile-bearing magma bodies (e.g. Arienzo et al., 2016).s

The magmas erupted at the PVD belong to a mildly K-enriched alkaline series ($Na_2O - 2 \leq K_2O$). Those of the Procida volcanic field are the least evolved, being mostly trachybasalt and shoshonite (D'Antonio et al., 2007), while the magmas erupted at the CF and Ischia volcanic fields have undergone complex magmatic evolution. The latter evolved from shoshonite through to trachyte or phonolite, and were affected by open-system evolution processes, such as mingling/mixing and crustal contamination, during periods of stagnation at variable depths during their ascent towards the surface (e.g., Orsi et al., 1995; Civetta et al., 1997; Signorelli et al., 1999; Pappalardo et al., 2002; Piochi et al., 2005; D'Antonio et al., 2007, 2022; Pabst et al., 2008; Tonarini et al., 2009; Arienzo et al., 2010, 2011, 2016; Pappalardo and Mastrolorenzo, 2012; Moretti et al., 2013; Fedele et al., 2016; Fedele, 2022). A combination of geophysical and petrological data highlights the existence of two main magma storage zones. The deeper zone is located at more than 8 km in depth (Zollo et al., 2008; Mangiacapra et al., 2008; Arienzo et al., 2016) whereas the shallower one is at ~ 4 km (De Siena et al., 2017; Arienzo et al., 2010; Voloschina et al., 2021).

Major- and trace-element data indicate that the Procida primitive K-basalts have a subduction-related isotopic signature, whereas all other PVD and Mount Somma-Vesuvio deposits also reveal a history of different magmatic processes that occurred in their plumbing systems (e.g., Tonarini et al., 2004; D'Antonio et al., 2007; Di Renzo et al., 2011).

Below is a brief description of the eruptions explored in this study and the volcanoes from which they erupted (see SM 1 for details).

- *The catastrophic caldera-forming eruptions of the CF volcanic field.* The eruptive and deformation history of the CF volcanic field is dominated by the Campanian Ignimbrite (CI; ~39 ka, Giaccio et al., 2017) and the Neapolitan Yellow Tuff (NYT; ~15 ka, Deino et al., 2004) caldera-forming eruptions (Orsi et al., 1996a). The CI eruption extruded ~300 km^3 of magma Dense Rock Equivalent (DRE) (Fedele et al., 2003), and comprises a complex event marked by an early Plinian phase that created a fallout deposit followed by the generation of voluminous pyroclastic density currents (PDCs) (Fisher et al., 1993; Rosi et al., 1999; Fedele et al., 2016; Moretti et al., 2019). The NYT eruption, the largest known trachytic phreato-Plinian event, extruded more than 40 km^3 of magma DRE (Orsi et al., 1992a, 1995; Wohletz et al., 1995). The caldera related to this eruption has been the site of intense volcanism and deformation since its formation and is currently the active portion of the CF caldera (Orsi et al., 1996a; Capuano et al., 2013).

- *The explosive eruptions of the post-NYT caldera*. Post-NYT volcanism has involved more than 70 eruptions within the NYT caldera, grouped into three periods of activity (Di Vito et al., 1999; Orsi et al., 2004, 2009; Smith et al., 2011). They are mostly phreatomagmatic eruptions, with some Plinian eruptions. The products of the magmatic Plinian phases (hereafter referred to ‘explosive eruptions’) of selected explosive events have been used for this study. The eruptions are Pomici Principali (PP; Fig. 1; 11,915 - 12,158 cal. yrs BP; 0.64 km^3 of erupted magma DRE), Agnano-Monte Spina (A-MS; Fig. 1; 4,482 - 4,625 cal. yrs BP; 0.85 km^3 of erupted magma DRE), Astroni 6 (As6; Fig. 1; 4,098 - 4,297 cal. yrs BP; 0.23 km^3 of magma DRE). Products from the Monte Nuovo (MN; Fig. 1; AD 1538; about 0.03 km^3 of magma DRE), the last and only historical eruption of the CF caldera, which occurred after about 3.5 ka of quiescence (Orsi et al., 2009), have also been analyzed.
- *Ischia volcanic field*. Volcanism at the island of Ischia began more than 150 ka BP. The eruptive and deformation history of the volcanic field has been deeply influenced by the high magnitude, caldera-forming Monte Epomeo Green Tuff eruption (~55 ka) (Vezzoli 1988; Orsi et al., 1991; Brown et al., 2008, 2014), during which a deep magma plumbing system developed (Moretti et al., 2013). The Cretaio Tephra (CT; Fig. 1; AD 430 cal. Age) extruded <0.02 km^3 of magma DRE and represents the highest magnitude eruption on the island in the last 10 ka (Orsi et al., 1992b, 1996b).
- *Procida*. The volcanic field of the island of Procida is located between the CF and the island of Ischia volcanic fields (Fig. 1b) and includes five monogenetic volcanoes. The erupted magmas of intermediate composition indicate that shallow

crustal magma chamber conditions were not established (De Astis et al., 2004; Mormone et al., 2011; Esposito et al., 2018). The last eruption formed the Solchiaro tuff ring (23,624 ± 330 cal. yrs BP; Morabito et al., 2014) and was fed by the most primitive magma ever erupted at both PVD and SVVC (D'Antonio et al., 2007).

3. Materials and Methods

The details of the materials and methods are provided in the Supplementary Material section (SM2). For the explosive eruptions, we analyzed pumice clasts from the earliest magmatic Plinian phase. However, for the CI caldera-forming eruptions, we also analyzed pumice clasts from the different PDC units.

Here, we provide details on the Cl geobarometer tool. Chlorine is a recognized geobarometer for alkaline magmas, providing estimates of the pressure of magma storage in shallow crustal reservoirs (Lowenstern, 1994; Balcone-Boissard et al., 2016). For fluid-saturated silicate melts, Cl preferentially partitions into the fluid phase rather than the melt, as shown by the pioneering work of Signorelli and Carroll (2000, 2002). At shallow depths (i.e., less than 210 MPa pressure equivalent at 1,000 °C; Anderko & Pitzer, 1993; Driesner and Heinrich, 2007), the components of the silicate melt-NaCl-H_2O pseudo-system are immiscible (Fig. 2a). The exsolved fluid phases include a H_2O-rich vapor phase and a Cl-rich brine. The composition and stability of the two-phase fluid depends on the silicate melt composition, temperature and pressure (Fig. 2a). This non-ideal fluid behavior is expressed by the Cl concentration in the silicate melt that is invariant or buffered when both vapor phase and brine are present, described by the Gibb's phase rule. The buffering effect on the Cl concentration in an alkaline silicate melt indicates an equilibrium between the melt and a two-phase fluid in the reservoir, at subsolvus conditions (Fig. 2a, b). At higher pressure, the silicate melt is in equilibrium with a vapor phase alone. In some magmas, Cl-bearing minerals such as apatite or feldspathoids, if present in sufficient quantity, could also be responsible for a Cl-buffering effect. Hereafter we refer to the Cl concentration resulting from such a buffering effect as the "Cl buffer value".

In this study, the Cl concentration in the residual glass (RG) has been measured for representative pumice clasts from each sampled fallout layer. Clast selection was based on the density measurements of a minimum of 100 pumice clasts per eruptive unit (Fig. 2b; Supplementary material SM3). Depending on the density distribution, the number of selected clasts was adjusted, totaling 3 to 7. Some coexisting MIs were also analyzed to fully describe the fluid saturation conditions of the magma: some MIs may have been entrapped before the buffering effect on Cl, when Cl was still demonstrating incompatible behavior (Balcone-Boissard et al., 2016). The presence of both vapor and brine led to the Cl-buffering effect on the silicate melt that is clearly preserved as residual glass of the eruptive products (Fig. 2b).

It is important to bear in mind that magma ascent may cause volatile degassing that may lead to micro-crystallization of the silicate melt. As rapid magma ascent may inhibit Cl partitioning into bubbles due to its low diffusivity in such differentiated melts, Cl may exhibit non-volatile behavior, leading to an increase in the Cl content by mass balance (Balcone-Boissard et al., 2009; Feisel et al., 2023). Thus, the Cl buffer value needs to be corrected for this degassing-induced crystallization effect (Tables 1, 2b Supplementary Material, SM3). The correction involves a manual decrease of the Cl buffer value by the percentage of degassing-induced microlites (which increases the Cl content through the mass balance effect), assuming that no Cl partitions into the microlites. The corrected Cl buffer value for the degassing-induced microlite content, if deemed necessary after textural investigations, is then representative of the reservoir conditions prior to eruption.

The challenge is then to convert the determined Cl buffer value into a pressure, namely the pressure of the last magma equilibration zone before eruption. For that purpose, there are two possibilities: i. using an experimentally determined Cl solubility law, where one exists for the studied sample composition, or ii. using a modelled Cl solubility law as developed by Webster et al. (2015). Most of the experimental determinations of Cl solubility use natural pumice clasts as starting material (Signorelli and Carroll, 2000, 2002). Each experimental Cl solubility law directly corresponds to a specific magma composition represented by a residual glass, and the application of the compositionally appropriate solubility law allows one to determine the pressure of equilibration of the magma based on the Cl buffer value, at a given temperature (Fig. 2c). The storage conditions of magmas with compositions for which the Cl solubility law has not been experimentally determined can still be defined from the Cl concentration in residual glass, using the Cl solubility model developed by Webster and collaborators (Webster et al., 2015). This model expresses the influence of each major and minor element (e.g., Si, Ti, Al, Mn, Fe, Mg, Ca, Na, K, and F) on Cl solubility through experimentally determined association coefficients. This approach takes into account the initial silicate melt composition and any associated changes in composition due to fractional crystallization, including subtle changes in melt composition. However, the results of recent experiments on both Cl solubility and Cl behavior in natural samples point out the more general role of S in the H-C-O-S-F-Cl system and how well this system describes the volatile behavior in alkali silicate melts (Webster et al., 2015). In particular oxidized S, when present, may substantially reduce the solubility of Cl in silicate melts at oxidizing conditions by modifying the extent to which it dissolves (Beermann et al., 2015; Botcharnikov et al., 2004; Webster et al., 2015, 2014). Therefore, the Cl concentration calculated using the model for a studied bulk melt composition, may also have to be corrected for the effect of oxidized S by reducing the modelled Cl solubility value by 30-40% relative (Webster et al., 2015, 2014). This effect can lead to underestimations of the storage pressure.

As discussed here, the presence of S has not yet been fully incorporated into the Cl solubility model (Webster et al., 2015), and this issue may introduce a bias between the pressure determined using this model versus that estimated with the compositionally relevant experimental Cl solubility law. When all parameters influencing Cl solubility in silicate melt are taken into consideration, application of both the Cl experimental solubility law and the Cl solubility model should give similar pressure estimates.

4. Results

4.1. Texture: phenocryst content and residual glass microcrystallinity

The different textures of the studied pumice clasts are best illustrated by the Back-Scattered Electron images (BSE; SM3 in Supplementary Material). The residual glass in the clasts has no visible sign of alteration. The pumice clasts of the CI fallout sequence are characterized by having few phenocrysts (<5 vol%; Signorelli et al., 1999) and a low microcrystallinity, while those of the NYT samples exhibit an even lower concentration of phenocrysts (<3 vol%; Orsi et al., 1995) and microlites in the groundmass. The products of magmatic Plinian phases of the explosive eruptions contain < 3 vol% phenocrysts, apart from those of the A-MS which are more porphyritic (5 – 10 vol%). Pumice clasts of the PP, A-MS and AS-6 eruption sequences display a microlite-free groundmass, and those of the AS-6 typically contain alternating highly and poorly vesiculated bands (Tonarini et al., 2009). CT pumice clasts (<5 vol% phenocrysts) contain vesicles with thin glassy walls with no microlites. MN pumice samples, in contrast, have a high microlite content (~30 vol%; Piochi et al., 2005) that is mostly composed of feldspars.

4.2. Residual glass composition: major elements and volatile (S and halogens - Cl, F) contents

The residual glass compositions of the analyzed pumice erupted at Campi Flegrei and Ischia display SiO_2 contents of between 57 and 63 wt% and alkali (Na_2O+K_2O) contents of between 11 and 15 wt%. Residual glass is thus either trachytic (A-MS, CT), or phonolitic (MN), or lies astride both compositions (PP, As6) (Fig. 3 and Tables 1, 2 in Supplementary Material). The residual glass of the samples of the Solchiaro eruption sequence displays a homogenous shoshonitic composition (e.g., 50.6-51.2 wt% SiO_2, 7.6-8.0 wt% Na_2O + K_2O, and 7.4-7.6 wt% CaO) (Fig. 3b, Table 1 in Supplementary Material). Within each eruption, the Cl content of the residual glass is constant, whereas F varies significantly (NYT: F = 0.19-0.28 wt%, Cl = 0.58 ± 0.02 wt%; PP: F = 0.18-0.29 wt%, Cl = 0.68 ± 0.02 wt%; A-MS: F = 0.24-0.41 wt%, Cl = 0.78± 0.03 wt%; As6: F = 0.19-0.25 wt%; Cl: 0.68 ± 0.02 wt%; MN: F = 0.50-0.60 wt%, Cl = 0.66± 0.02 wt%; CT: F = 0.19-0.36 wt%, Cl = 0.55 ± 0.01 wt%) (Fig. 4). The CI fallout deposits have similar F contents (0.35-0.46 wt%) throughout, and Cl values that vary with stratigraphic height (base: 0.90 ± 0.02 wt%; middle: 0.84 ± 0.01 wt%; top: 0.78 ± 0.02 wt%) (Fig. 5). Pumice samples collected from the voluminous, stratigraphically overlying PDC deposits show large variations in Cl concentrations (from 0.01 up to ~1 wt%) (Supplementary Material SM4). For six of the investigated eruptions (CI, NYT, PP, As6, MN, and CT), S has also been measured (Fig. 6). The RESIDUAL GLASS shows S contents below the detection limit (80 ppm) for CT and

MN and mean S up to 500 ± 126 ppm for NYT, 104 ± 14 ppm for CI and less than ~300 ± 65 ppm for both PP and As-6. For Solchiaro, F and Cl contents span restricted ranges of 0.09 - 0.15 wt% and 0.17-0.18 wt%, respectively (Table 1 in Supplementary Material), while S has not been measured.

4.3. Melt inclusion (MI) composition: major elements and volatile (S and halogens - Cl, F) contents

S contents of some melt inclusions in crystals from the CI (pyroxenes), NYT (magnetites) and CT (magnetites) have been analyzed. The MIs trapped in magnetite from the NYT show the highest S concentration (603 ± 30 ppm). Those from the CT feldspars extracted from the whole eruption sequence display an S content (250 ± 40 ppm) similar to the mean value for CI (252 ± 64 ppm). The presence of anhedral iron sulphide in CT and NYT eruptions, 10 to 50 µm in diameter, trapped in magnetite and containing 33.7 ± 1.5 wt% of S, indicates a high S concentration in the melt that precipitates out into sulphides (Table 2a in Supplementary Material).

5. Discussion

5.1 Volatile (halogen, S) content of the melts feeding the investigated eruptions

Halogen (F and Cl) and S contents in both residual glass and melt inclusions have rarely been reported in the literature (Arienzo et al., 2010, 2016; Fourmentraux et al., 2012; Moretti et al., 2013; Balcone-Boissard et al., 2016; D'Augustin et al., 2020). The available F and Cl contents detected in both residual glass and melt inclusions of the A-MS samples support the use of Cl as a geobarometer on the basis of the model developed for the SVVC magmas (Fig. 2; Balcone-Boissard et al., 2016). The NYT and CI pre-eruption melts trapped in melt inclusions show the highest S concentration of all the studied eruptions, as well as the largest difference between pre-eruption and post-eruption contents. The CT pumice clasts have moderate S contents in the melt inclusions (250 ± 40 ppm) and completely degassed residual glass (below the detection limit of 80 ppm), although the presence of iron sulphide blebs (33.7 ±1.5 wt% of S) suggests a higher S concentration. The S content is low (~170 ± 65 ppm) in the residual glass of the PP and As-6 samples, and below the detection limit in the residual glass of MN (no melt inclusion data have been acquired for PP, As-6 and MN samples).

The F (0.09 - 0.15 wt%) and Cl (0.17 - 0.18 wt%) contents of the Solchiaro basic residual glass (Table 1 in Supplementary Material) are lower than those of the other studied eruptions, although they are in accordance with the less differentiated composition of the glass. They are lower than the measured volatile content in melt inclusions in olivines, with F up to 0.2 wt%, Cl up to 0.45 wt%, and S of 0.17 wt% (Esposito et al., 2011). It is hard to compare residual glass and melt inclusion data from literature as the detailed study on MI span a large range of volatile contents, resulting in melt entrapment under volatile saturation at different depths and times in the magma plumbing system. Here, we consider Solchiaro magma as an adequate parental end-member of the PVD (Mormone et al., 2011): the measured residual glass composition can thus be interpreted as being the volatile content for a step of fractional crystallization of a fluid-undersaturated magma (Fig. 2b; Balcone-Boissard et al., 2016).

5.2 Cl buffer value, S effect and magma equilibrium pressure

5.2.1 Cl buffer value

The growth of Cl-bearing minerals in a silicate melt is one of the possible processes that can buffer the Cl concentration of the residual glass. However, the investigated pumice clasts do not contain Cl-rich phenocrysts or microlites, and the residual glass is not highly microcrystalline, apart from in samples from the MN eruption. The Cl-rich mineral phases found at Campi Flegrei are sodalite, fluorite, apatite and biotite; but they occur as rare microlites, even in the highly crystallized residual glass of the later phase products of the MN eruption (Melluso et al., 2012; Arzilli et al., 2016). Sodalite occurs in a small quantity, preventing it from affecting the Cl concentration in the residual glass. Therefore, the constant Cl values do not represent a buffered melt value due to crystallization of a condensed phase. Nevertheless, in the case of the highly microcrystalline residual glass of MN, the melt composition may have been modified by degassing-induced crystallization: we circumvent this effect on Cl solubility using the experimental Cl solubility law. We applied a mass-balance correction to the Cl concentration of the MN samples, due to the presence of 30% of feldspar microlites (Piochi et al., 2005; this work). For all the other cases, the constant Cl value measured in the residual glass was assumed to be the Cl value buffered by the fluid assemblage (vapor + brine).

5.2.2 The question of S in the PVD magmas

The geochemical and isotopic features of the PVD rocks erupted over the past 15 ka differ from those erupted earlier. The detected differences have been partly attributed to an increase in crustal contamination through time (Pappalardo et al., 2002; D'Antonio et al., 2007; Di Renzo et al., 2011). Sulfur is an incompatible element for the major crystalline phases, except for iron sulphide blebs occurring in magnetite, and its solubility is pressure-, temperature- and oxygen fugacity-dependent (Carroll and Webster, 1994). CO_2 flushing via fluids released from deeper parental magmas (Mangiacapra et al., 2008; Moretti et al., 2013), rather than an unlikely contribution of the limestone bedrock (D'Antonio, 2011), can decrease the H_2O content in the melt, and may allow for enhanced exsolution of S in the melt (as the magma becomes less hydrous, its sulphide saturation will decrease and potentially lead to the generation of an immiscible sulphide phase (Fortin et al., 2015)

Such exsolution processes may occur in the pre-eruptive magma of the NYT and later explosive eruptions. Thus, using the Cl solubility model we have to take this into account and manually introduce the effect of S on Cl solubility. Conversely, the S content of CI and NYT is similar, supported by data from the literature and the climatic impact of CI (Fedele et al., 2005, 2007). No S-effect correction using Cl modelling solubility is required to explain the Cl signature of CI melts since the experimental Cl solubility law determined using the CI composition wholly describes the volatile interactions, in particular the S effect on Cl solubility.

5.2.3. *Magma storage pressure*

5.2.3.1 The magmatic Plinian phase of the explosive eruptions of Campi Flegrei and Ischia volcanic fields

For the trachytic A-MS and CT and the phonolitic MN eruptions, the Cl solubility law available for each of these compositions (Signorelli and Carroll, 2000, 2002) and the Cl solubility model (Webster et al., 2015) with the S correction, yield the same magma storage pressure : 65 ± 10 MPa and 140 ± 5 MPa for the trachytic A-MS and CT eruptions, respectively (Fig. 7c), and 115 ± 10 MPa for the phonolitic MN one (Fig. 7d). For the As6 and PP eruptions, the magma pressure domain is the same, since they were fed by magmas with the same composition and exhibit the same Cl buffer value (Figs. 3, 4). As the Cl solubility curves for trachytic and K-phonolitic melts are close to one another, the pressure domain is quite narrow, at between 95 and 110 MPa. The pressure values estimated using the Cl solubility model with the S correction are 90 and 110 MPa for As6 and PP, respectively (Fig. 7c). Thus, both the Cl solubility law and the solubility model methods provide the same pressure estimates when the S correction is applied to the modelling (Fig. 8).

5.2.3.2 Caldera-forming eruptions of CF

The samples of the basal fallout sequence of the CI display three different Cl buffer values, depending on their position in the stratigraphic sequence, hence on the timing of magma withdrawal (base: 0.90 ± 0.02 wt%; middle: 0.84 ± 0.01 wt%, top: 0.78 ± 0.02 wt%, Fig. 4b. These Cl values, which are the highest found in the RESIDUAL GLASS of all the analyzed pumice clasts of the PVD, decrease upwards through the sequence, with each stratigraphic level clearly showing a specific Cl buffer value. The Cl solubility law has been experimentally determined specifically for the CI composition (Signorelli and Carroll, 2002) (Fig. 7a), making it possible to assess the magma equilibration pressure prior to the Plinian phase. The trachytic magma body formed a shallow apex with its top at 30 ± 5 MPa. The pressures are also recorded by the compositionally intermediate and poorly evolved CI products (45 ± 5 MPa, and 65 ± 5 MPa, respectively). These differentially evolved magmas generated the lowermost, the intermediate and the uppermost portions of the fallout sequence, respectively (Fig. 7a). The same pressures have also been estimated using the Cl solubility model. It is worth stressing that the correspondence between the results of the two methods can be only achieved without an S correction. The Cl contents have also been determined for a few samples from the PDC deposits of the CI eruption sequence. The large variability of the obtained results is incompatible with a fluid-buffered effect and could instead arise from degassing processes or scavenging of Cl by zeolites (Cappelletti et al., 2003). Post-eruptive degassing processes are common in such voluminous deposits that remain at high temperature for a long time after deposition. The magma corresponding to the PDC phase may also inherit various geochemical signatures from a chemically and isotopically distinct batch of magma that recharged sometime before eruption (Arienzo et al., 2009).

For the NYT, the residual glass covers a large range of composition, straddling the phonolite and trachyte fields (Fig. 3). Consequently, the pressure domain deduced from the residual glass composition is large too, between 130 and 165 MPa, using the experimental Cl solubility law determined for both the trachytic and phonolitic melts (Fig. 7b). Considering the significant S content in the NYT magma, its influence on Cl solubility must be taken into account (Fig. 6); therefore, a 35% relative correction of the Cl buffer value has been applied using the Cl solubility model, yielding a pressure value of ~120-130 MPa, which is close to the pressure domain estimated using the Cl solubility laws.

5.3 Architecture of the magmatic plumbing systems

The results for magma storage pressures can be discussed in the light of our current knowledge of the magmatic feeding systems of Neapolitan volcanoes and their intimate relationships with magma eruption dynamics (Fig. 9) (Arienzo et al., 2010, 2016; Moretti et al., 2013; Astbury et al., 2018). The studied fallout deposits of the CI and NYT eruptions account for a minor proportion of the entire eruptive sequences, thus representing only a small portion of the total extruded magma. Those of the smaller volume explosive eruptions

(<1 km^3 of magma; PP, AM-S, As6 and MN at Campi Flegrei and CT at Ischia), represent variable and relatively large portions of the total emitted magmas.

For the magmatic Plinian phase of the CI, a low but progressively increasing pressure of 30 ± 5 to 65 ± 5 MPa has been obtained using both methods for establishing Cl buffering values. This applies to the stratigraphically lowermost portion of the CI eruption sequence produced by the accumulation of products representative of the most evolved magma equilibrating with Cl at low pressure. This pressure range cannot be extrapolated to the storage conditions of the total volume of magma extruded during the course of the entire event since it is only relevant for the earliest extruded magma. Indeed, the huge ca. ~300 km^3 volume of magma could not be stored at such a shallow depth. Conversely, this portion may represent a shallow, resident magma later intercepted by the least evolved, ascending CI magma (Di Salvo et al., 2020). Unfortunately, no pressure data have been obtained for the poorly evolved CI melts (not erupted) that possibly differentiated at variable depths during ascent from the deeper zone, located beneath 8 km depth, to the shallower one. Moreover, no pressure data have been calculated for the PDC deposits as volatile (H_2O and F, Cl) contents are dominated by post-deposition degassing processes and the growth of zeolites (Cappelletti et al., 2003) which can entrap Cl. The very low-pressure values obtained contrast with the high storage pressures that characterize the magma producing the later PDCs (e.g. Moretti et al., 2019) but they do provide constraints on the architecture of the shallowest equilibration zone of the magma plumbing system prior to the CI eruption.

The depth at which magma bodies form is controlled by volatile exsolution and crustal rheology. At pressures > 250 MPa, the viscosity of the crust in long-lived magmatic provinces is sufficiently low to inhibit most eruptions (Huber et al., 2019). Conversely, magma chamber growth at lower pressure (<150 MPa) is inhibited due to a combination of the exsolution of a volatile phase and high evacuation rates, and the crust being more viscous and brittle. However, a long-lived system can accumulate magma and build up reservoirs in the lower crust thanks to the long duration of intrusions (Karakas et al., 2017). Such a modification to the lower crustal zone impacts the upper portion of the crust, by modifying the thermal budget and thus reducing the flux of magma required to sustain a shallow magma reservoir. Here it can be inferred that the upper crust was mechanically and thermally able to relax, allowing the formation of shallower, less voluminous magma bodies. Such low pressure magma bodies are only transient, and unable to grow to a significant size, as they quickly erupt if recharged by fresh magma (Huber et al. 2019).

The greatest portion of the CI magma was likely stored at higher pressure than that of the batch feeding the Plinian phase. The latter, with an estimated volume of ~12 km^3, likely formed a vertically extended apex at pressures of 30 to 65 MPa. In this situation, the upper crust is able to host a growing magma body.

Our results are in accordance with the model proposed by Marianelli et al. (2006), based on the volatile content of melt inclusions. The authors suggest a decompression event from the deepest reservoir located at 150 MPa, down to 50 MPa, representing the upward movement of the trachytic magma into the crust. This may correspond to the potentially large, eruptible and long-lived magma bodies expected beneath volcanoes (Huber et al., 2019). Fanara et al. (2015), based on volatile content of residual glass measured on natural samples and estimated experimentally, also suggested a similar structure with two magma reservoirs located at different levels: a deeper one at about 8 to 15 km and a shallower one at 1 to 8 km. The occurrence of a vertical apex of the magma chamber is justified by the strong correlation between the pressure values estimated from the Cl buffering effect and stratigraphic heights of the analyzed samples. This apex would have been formed following a possible pressure build-up of the reservoir, by a magma intrusion from the deeper part of the system. This scenario can explain the unrest phases at CF which could be driven by small portions of un-eruptible magma located at shallow depth (De Siena et al., 2010). There are two main hypotheses to account for the shallow depth of the earliest erupted magma. The first is linked to the tectonic setting of the PVD: the most evolved magma batch, located at the top of the larger chamber with a mean depth of about 8 km, intruded a dense network of fractures and faults that are related to the regional NE-SW and NW-SE structural systems. The Plinian phase of the eruption was fed by a central vent formed in a discrete sector of this vertically extensive, uppermost portion of the reservoir. These faults then controlled the eruption-related collapse of the caldera (Orsi et al., 1996a; Moretti et al., 2013). The other hypothesis is to consider the crustal magma plumbing system as being made of transient portions of magma stored at different depths. The uppermost reservoirs, with the most evolved trachytic magma, only correspond to a small part of the magma involved in the Plinian phase, which was able to be recharged several times (Di Salvo et al., 2020). When the eruption began, the decompression destabilized the magma stored within a larger reservoir at greater depth, following a volatile saturation event or intrusion of a more mafic, high-temperature magma (Arienzo et al., 2009, 2011; Di Salvo et al., 2020). The transient nature of the shallowest magma found here is in accordance with the effects of crustal rheology.

The NYT caldera-forming eruption extruded 40 km^3 of magma. The pressure/depth of the magma emitted during the Plinian events with trachytic-phonolitic compositions has been evaluated using the two methods, giving a minimum pressure of 130 MPa for the top of the reservoir. This location for the NYT magma reservoir is in agreement with the hypothesized top of the reservoir at about 4 km determined by modelling of the thermal regime of the CF magmatic system (Di Renzo et al., 2016).

The results for the residual glass of the A-MS eruption suggest a magma reservoir located at a pressure of 65 MPa, perhaps inherited from the NYT eruption (de Vita et al., 1999). This pressure value is slightly lower, implying a shallower depth, than that proposed by Arienzo et al. (2010) based on melt inclusion geobarometry. These authors also showed that two superimposed reservoirs were evacuated during the eruption and that deep CO_2-flushing occurred. The CO_2 may have played a significant role by dehydrating the magma and by modifying the H_2O-Cl equilibrium. Thus, the magma storage pressure might have been higher than that deduced here from the Cl buffering effect.

The pressures of the magmatic reservoirs feeding the PP and As6 eruptions have been estimated at similar values of 95-110 MPa, while the storage pressure for the magma feeding the MN eruption has been estimated at 115 MPa using the Cl solubility method. This estimate is similar to the value of 150 MPa defined by Piochi et al. (2005) on the basis of geochemical modelling of H_2O solubility in magma (MELTS). Such a depth is in agreement with the reconstruction made by Di Vito et al. (2016) based on the historical, archaeological and geological record of the Campi Flegrei caldera. The authors estimated the surface deformation preceding the Monte Nuovo eruption and investigated the shallow magma transfer. Data suggest progressive magma accumulation in a source c.a. 5 km below the caldera center, and its transfer to a depth of c.a. 4 km below Monte Nuovo.

The pressure of the storage zone of the magma feeding the CT eruption, the only event on Ischia that has been studied here, is 140 MPa, a value that falls within those evaluated by Moretti et al. (2013b). These authors suggested a composite plumbing system beneath Ischia including magma storage zones located at various depths, the shallowest of which is at 100-160 MPa.

The pressure estimates evaluated using the Cl barometer are extremely shallow, compared to most previous estimates of magma storage depths in the CF region obtained using other techniques (e.g., melt inclusions, geophysics). The results indicate the vapor-melt equilibration of ephemeral magma ponding zones at shallow depth within a dynamic magma plumbing system. Beyond the stable magma reservoir located below a depth of 8 km, multiple magma ponding zones may have transiently formed at shallower depths at least during the past 10 – 15,000 years (Pabst et al., 2007).

In addition to the interpretations of the CF plumbing system discussed here (Fig. 9), Fourmentraux et al. (2012) have published work on the volatile behavior of the magma feeding the Averno 2 eruption (di Vito et al., 2011). They pointed out that two independent batches of magma rose through vertical fractures at the periphery of the NYT caldera. In particular, H_2O and Cl data indicate a storage pressure of 25 MPa for the shallowest and most-differentiated erupted magma. This magma thus represents the shallowest depth of those that have erupted over the past 15 ky at the CF, which probably formed just a short time prior to eruption.

5.4. Pre-eruptive water contents

As a corollary to the pressure and depth constraints presented here for magmas feeding the selected PVD eruptions, the maximum pre-eruptive H_2O content for these silicate melts has also been estimated (Fig. 9). Such estimates can be performed if the H_2O solubility law for the composition of the erupted magma is known. Water concentrations were estimated using a H_2O solubility law for the composition of the melt corresponding to the pressure deduced from the Cl-buffering effect (Fig. 9, 10). However, this approach ignores the influence of other volatiles (mainly CO_2 and S) on H_2O solubility, as experimental H_2O solubility laws do not generally take them into account. The obtained results suggest H_2O contents of ~4 wt% for phonolitic (MN eruption), and between 1.5 and 6.5 wt% for trachytic magmas. These represent maximum values, because the presence of CO_2 could depress the amount of water dissolved in melt at saturation by lowering the solubility limit of water, which would lead to Cl extraction from the melt (Botcharnikov et al., 2007). It is also likely that there could be significant CO_2 fluxing through shallow magma chambers at PVD. CO_2 fluxing closely linked to deep supercritical CO_2-rich fluids partly controls eruption dynamics (Moretti et al., 2013; Moretti et al., 2019). This process, due to a decrease in H_2O solubility induced by increasing CO_2 fugacity of the fluid phase, could also enhance volatile saturation in the magma, increasing the amount of exsolved fluids. The minimum exsolved H_2O content during magma ascent can be estimated using the H_2O content in melt inclusions. In several cases, the H_2O contents measured in melt inclusions are consistent with our estimates (Fig. 10). The water content determined for the A-MS eruption has values of between 0.85 and 3.05 wt% (Arienzo et al., 2010), providing a relatively good match for the value of 4 wt% obtained using the H_2O solubility law. For the CI eruption, H_2O contents of 2 - 3 wt% were found for the shallow portion of the reservoir (Marianelli et al., 2006; Moretti et al., 2019), in agreement with the value (1.5 - 2 wt%; Fig. 10) determined using the solubility law. These data describe the H_2O content (from 0.83 ± 0.07 to 3.74 ± 0.06 wt%) for the trachytic magmas emitted during the CI eruption, as measured in melt inclusions by Fanara et al. (2015).

5.5. Comparison with the eruptions of Somma-Vesuvio Volcanic Complex and other alkali-rich systems

Previous researchers have highlighted a long-lived common pool of magma located at 8-10 km depth beneath the Campanian volcanoes (Pappalardo and Mastrolorenzo, 2012; Zollo et al., 2008) and the possibility of coupled deformation in recent times (uplift and subsidence at PVD and SVVC are correlated; Walter et al., 2014). This link could be due to a possible migration of magmatic fluids from depth: upward migration of magma causes pressure changes within magma or hydrothermal fluid reservoirs, which causes ground deformation that can be measured as displacement at the surface, as at both the PVD and SVVC given that the two complexes are geographically close to each other (Gonnermann et al., 2012; Freymuller et al., 2015). Several geochemical studies on melt inclusions have demonstrated that magma storage occurred at depths of 3-5 km and 8-10 km (e.g., Scaillet et al., 2008), with an upward migration of the magma chamber through time. Using the same method as in the present work, Balcone-Boissard et al. (2016) highlighted two main magma ponding zones at 180 - 200 MPa and 100 MPa, with a still shallower reservoir at less than 50 MPa feeding the most recent eruptions since AD 1822. This also correlates with a different magma composition, with the shallowest and most recent eruptions displaying a Strombolian eruptive style involving a less differentiated melt (tephritic). However, unlike the PVD, no short-lived shallow magma apophyses have been identified at SVVC; the PVD is mainly composed of a nested caldera with specific unrest signals.

The buffering effect on Cl is also found at other volcanic systems involving alkali-rich rhyolitic magmas, such as Pantelleria (Green Tuff eruption) or the East African Rift (Gedemsa and Corbetti volcanoes, Ethiopia; *unpublished data*). This shows that geobarometric constraints can be calculated with Cl for differentiated alkali-rich magmas, including not only trachyte or phonolite but also rhyolite, and occurring in various geodynamic contexts.

6. Implications

One of the most important results of this work is that Cl can be used as a geobarometer for alkaline magmas. The identified Cl buffering effect of fluid-melt interaction allows the shallowest depth at which fluid-melt equilibrium occurs with respect to Cl to be calculated.

DOI: https://doi.org/10.2138/am-2022-8883. http://www.minsocam.org/

Secondly, these results have major implications for the architecture of the plumbing system through time: the upper part of the plumbing system has varied in depth through time (Fig 10), thus corroborating the hypothesis of a dynamic multi-depth plumbing system and the idea that its architecture has been dictated by both the regional and local structural setting, fluid saturation, and the thermal regime of the magmatic area. Such extremely shallow, short-lived magma bodies in the upper crust will not necessarely lead to an eruption if the feeder system from the deepest reservoir is not maintained, or if the injection frequency is too low, in which case the magmas will cool fast and crystallize before building up a magmatic reservoir of sufficient size to erupt.

This approach can be used for other volcanic systems fed by alkali-rich magmas. By systematic application to past eruptions of a given volcanic center, it could provide useful constraints on the architecture of polybaric plumbing systems, seen as being made up of a several magma ponding zones through the entire crust.

Finally, this study also highlights the importance of studying the magmatic fluid phase as a complex C-H-O-S-F-Cl system, with interactions and feedback between different fluid and melt species.

Acknowledgments

We thank M. Fialin, F. Couffignal, N. Rividi for support at the electronic microprobe (Camparis, Paris, France) and O. Boudouma for textural analyses by SEM (Paris, France). A. Carandente, P. Belviso and P. Petrosino helped in sampling fallout deposits. This work was performed as part of VINCI program (Université Franco-Italienne).

References

Anderko, A., and Pitzer, K.S. (1993) Equation-of-state representation of phase equilibria and volumetric properties of the system NaCl-H_2O above 573 K. Geochimica and Cosmochima. Acta 57, 1657–1680. doi:10.1016/0016-7037(93)90105-6

Andújar, J. and Scaillet, B. (2012). Relationships between pre-eruptive conditions and eruptive styles of phonolite-trachyte magmas. Lithos, 2012, 152 (1), pp.122-131.

Arienzo, I., Civetta, L., Heumann, A., Wörner, G., Orsi, G. (2009) Isotopic evidence for open system processes within the Campanian Ignimbrite (Campi Flegrei–Italy) magma chamber. Bulletin of Volcanology 71, 285–300. https://doi.org/10.1007/s00445-008-0223-0

Arienzo, I., Moretti, R., Civetta, L., Orsi, G., Papale, P. (2010) The feeding system of Agnano-Monte Spina eruption (Campi Flegrei, Italy): Dragging the past into present activity and future scenarios. Chemical Geololgy, 270, 135–147. doi:10.1016/j.chemgeo.2009.11.012

Arienzo, I., Heumann, A., Wörner, G., Civetta, L., Orsi, G. (2011) Processes and timescales of magma evolution prior to the Campanian Ignimbrite eruption (Campi Flegrei, Italy), Earth and Planetary Science Letters, Volume 306, Issues 3–4, Pages 217-228, https://doi.org/10.1016/j.epsl.2011.04.002

Arienzo,I., Mazzeo, F.C., Moretti, R., Cavallo, A., D'Antonio, M. (2016) Open-system magma evolution and fluid transfer at Campi Flegrei caldera (Southern Italy) during the past 5ka as revealed by geochemical and isotopic data: The example of the Nisida eruption, Chemical Geology, Volume 427, Pages 109-124, https://doi.org/10.1016/j.chemgeo.2016.02.007

Arzilli, F., Piochi, M., Mormone, A., Agostini, Dr, Carroll, M. (2016) Constraining pre-eruptive magma conditions and unrest timescales during the Monte Nuovo eruption (1538 AD; Campi Flegrei, Southern Italy): integrating textural and CSD results from experimental and natural trachy-phonolites. Bulletin of Volcanology. 78. 10.1007/s00445-016-1062-z.

Astbury, R.L., Petrelli, M., Ubide, T., Stock, M.J., Arienzo, I., D'Antonio, M., Perugini, D. (2018) Tracking plumbing system dynamics at the Campi Flegrei caldera, Italy: High-resolution trace element mapping of the Astroni crystal cargo, Lithos, Volumes 318–319, Pages 464-477, https://doi.org/10.1016/j.lithos.2018.08.033

Bachmann, O. and Huber, C. (2016). Silicic magma resevoirs in the Erath's crust. American Mineralogist, 101, 2377-2404.

Balcone-Boissard, H., Boudon, G., Cioni, R., Webster, J.D., Zdanowicz, G., Orsi, G., Civetta, L. (2016) Chlorine as a geobarometer for alkaline magmas: Evidence from a systematic study of the eruptions of Mount Somma-Vesuvius. Scientific Report, 6, 21726. doi:10.1038/srep21726

Balcone-Boissard, H., Baker , D.R., Villemant , B., Boudon, G. (2009) F and Cl diffusion in in phonolitic melts : Influence of the Na/K ratio. In D.R. Baker, A. Aiuppa and J. Webster. Halogens in Volcanic Systems and Their Environmental Impacts, Chemical Geology, pp.89-98, 263.

Beermann, O., Botcharnikov, R.E., Nowak, M. (2015) Partitioning of sulfur and chlorine between aqueous fluid and basaltic melt at 1050°C, 100 and 200MPa. Chemical Geology, 418, 132–157. doi:10.1016/j.chemgeo.2015.08.008

Berthod, C., Médard, E., Bachèlery, P. et al. (2021). The 2018-ongoing Mayotte submarine eruption: Magma migration imaged by petrological monitoring, Earth and Planetary Science Letters, Volume 571, 117085, https://doi.org/10.1016/j.epsl.2021.117085.

Blundy, J.D., Cashman K.V. (2008). Petrologic Reconstruction of Magmatic System Variables and Processes. Reviews in Mineralogy and Geochemistry 69(1):179-239, DOI:10.2138/rmg.2008.69.6

Bonafede, M., Amoruso, A., Crescentini, L., Gottsmann, J.H., Todesco, M., Trasatti, E. (2022) Source modelling from ground deformation and gravity changes at the Campi Flegrei Caldera, Italy. In: Orsi, G., D'Antonio, M., Civetta, L. (eds) Campi Flegrei. Active Volcanoes of the World. Springer, Berlin, Heidelberg.

Botcharnikov, R.E., Behrens, H., Holtz, F., Koepke, J., Sato, H. (2004) Sulfur and chlorine solubility in Mt. Unzen rhyodacitic melt at 850 °C and 200 MPa. Chemical Geology, 213, 207–225. doi:10.1016/j.chemgeo.2004.08.044

Botcharnikov, R.E., Holtz, F., Behrens, H. (2007) The effect of CO_2 on the solubility of H2O-Cl fluids in andesitic melt. European Journal of Mineralogy, 19, 671–680. doi:10.1127/0935-1221/2007/0019-1752

Bower, S. M. and Woods,A. W. (1998). On the influence of magma chambers in controlling the evolution of explosive volcanic eruptions, Journal of Volcanology and Geothermal Research, Volume 86, Issues 1–4, Pages 67-78, https://doi.org/10.1016/S0377-0273(98)00081-X.

Cappelletti, P., Cerri, G., Colella, A., de'Gennaro, M., Langella, A., Perrotta, A., Scarpati, C. (2003) Post-eruptive processes in the Campanian Ignimbrite. Mineralogy and Petrology, 79, 79–97. doi:10.1007/s00710-003-0003-7

Carroll, M.R., and Webster, J.D. (1994) Solubilities of sulfur, noble gases, nitrogen, chlorine, and fluorine in magmas. Rev. Mineral. Geochemistry 30, 231–280.

Cashman, K., Sparks, S., Blundy, J. (2017) Vertically extensive and unstable magmatic systems: A unified view of igneous processes. Science. 355. eaag3055. 10.1126/science.aag3055.

Chiodini, G., Vandemeulebrouck, J., Caliro, S., D'Auria, L., De Martino, P., Mangiacapra, A., Petrillo, Z., (2015) Evidence of thermal-driven processes triggering the 2005–2014 unrest at Campi Flegrei caldera. Earth and Planetary Science Letter, 414, 58–67. doi:10.1016/j.epsl.2015.01.012

Civetta, L., Orsi, G., Pappalardo, L., Fisher, R.V., Heiken, G., Ort, M. (1997) Geochemical zoning, mingling, eruptive dynamics and depositional processes — the Campanian Ignimbrite, Campi Flegrei caldera, Italy. Journal of Volcanology and Geothermal Research, 75, 183–219. doi:10.1016/S0377-0273(96)00027-3

D'Antonio, M., Tonarini, S., Arienzo, I., Civetta, L., Renzo, V. Di (2007) Special Paper 418: Cenozoic Volcanism in the Mediterranean Area, Geological Society of America Special Papers. Geological Society of America. doi:10.1130/978-0-8137-2418-8

d'Antonio, M. (2011) Lithology of the basement underlying the Campi Flegrei caldera: Volcanological and petrological constraints, Journal of Volcanology and Geothermal Research, Volume 200, Issues 1–2, Pages 91-98, https://doi.org/10.1016/j.jvolgeores.2010.12.006.

D'Auria, L., Pepe, S., Castaldo, R., Giudicepietro, F., Macedonio, G., Ricciolino, P., Tizzani, P., Casu, F., Lanari, R., Manzo, M., Martini, M., Sansosti, E., Zinno, I. (2015) Magma injection beneath the urban area of Naples: a new mechanism for the 2012–2013 volcanic unrest at Campi Flegrei caldera. Scientific Report, 5, 13100. doi:10.1038/srep13100

De Astis, G., Pappalardo, L., Piochi, M. (2004). Procida volcanic history: new insights into the evolution of the Phlegraean Volcanic District (Campania region, Italy). Bulletin of Volcanology, 66, 10.1007/s00445-004-0345-y.

De Siena, L., Del Pezzo, E., Bianco, F. (2010) Seismic attenuation imaging of Campi Flegrei: Evidence of gas reservoirs, hydrothermalbasins, and feeding systems. Journal of Geophysical Research, 115, B0931

De Siena, L., Amoruso, A., Pezzo, E. D., Wakeford, Z., Castellano, M., & Crescentini, L.

(2017). Space-weighted seismic attenuation mapping of the aseismic source of Campi Flegrei 1983–1984 unrest. Geophysical Research Letters, 44, 1740–1748. https://doi. org/10.1002/2017GL072507

Deino, A.L., Orsi, G., De Vita, S., Piochi, M. (2004) The age of the Neapolitan Yellow Tuff caldera-forming eruption (Campi Flegrei caldera – Italy) assessed by 40Ar/39Ar dating method. Journal of Volcanology and Geothermal Research, 133, 157–170. doi:10.1016/S0377-0273(03)00396-2

Di Matteo, V., Carroll, M.R., Behrens, H., Vetere, F., Brooker, R.A. (2004) Water solubility in trachytic melts. Chemical Geology, 213, 187–196. doi:10.1016/j.chemgeo.2004.08.042

Di Renzo, V., Arienzo, I., Civetta, L., D'Antonio, M., Tonarini, S., Di Vito, M.A., Orsi, G. (2011) The magmatic feeding system of the Campi Flegrei caldera: Architecture and temporal evolution. Chemical Geology, 281, 227–241. doi:10.1016/j.chemgeo.2010.12.010

Di Renzo, V., Wohletz, K., Civetta, L., Moretti, R., Orsi, O., Gasparini, P. (2016) The thermal regime of the Campi Flegrei magmatic system reconstructed through 3D numerical simulations, Journal of Volcanology and Geothermal Research, Volume 328, Pages 210-221, https://doi.org/10.1016/j.jvolgeores.2016.11.004.

Di Salvo, S., Avanzinelli, R., Isaia, R., Zanetti, A., Druitt, T., Francalanci,L. (2020) Crystal-mush reactivation by magma recharge: Evidence from the Campanian Ignimbrite activity, Campi Flegrei volcanic field, Italy, Lithos, Volumes 376–377, 105780, https://doi.org/10.1016/j.lithos.2020.105780

Di Vito, M.A., Arienzo, I., Braia, G., Civetta, L., D'Antonio, M., Di Renzo, V., Orsi, G. (2011) The Averno 2 fissure eruption: a recent small-size explosive event at the Campi Flegrei Caldera (Italy). Bulletin of Volcanology, 73, 295–320.

https://doi.org/10.1007/s00445-010-0417-0

Driesner, T., and Heinrich, C.A. (2007) The system H2O–NaCl. Part I: Correlation formulae for phase relations in temperature–pressure–composition space from 0 to 1000°C, 0 to 5000bar, and 0 to 1 XNaCl, Geochimica et Cosmochimica Acta, Volume 71, Issue 20, Pages 4880-4901, https://doi.org/10.1016/j.gca.2006.01.033.

Edmonds, M., and Woods, A. W. (2018). Exsolved volatiles in magma reservoirs. *J. Volcanol. Geotherm. Res.* 368, 13–30. doi:10.1016/j.jvolgeores.2018.10.018

Esposito, R., Bodnar, R.J., Danyushevsky, L. V., De Vivo, B., Fedele, L., Hunter, J., Lima, A., Shimizu, N. (2011) Volatile evolution of magma associated with the solchiaro eruption in the Phlegrean Volcanic District (Italy). Journal of Petrology 52, 2431–2460. doi:10.1093/petrology/egr051

Esposito, R., Badescu, K., Steele-MacInnis, M., Cannatelli, C., De Vivo, B., Lima, A., Bodnar, R.J., Manning, C.E. (2018) Magmatic evolution of the Campi Flegrei and Procida volcanic fields, Italy, based on interpretation of data from well-constrained melt inclusions, Earth-Science Reviews, 185, Pages 325-356, https://doi.org/10.1016/j.earscirev.2018.06.003.

Fanara, S., Botcharnikov, R.E., Palladino, D.M., Adams, F., Buddensieck, J., Mulch, A., Behrens, H. (2015) Volatiles in magmas related to the Campanian Ignimbrite eruption : Experiments vs . natural findings. American Mineralogist, 100, 2284–2297. doi:10.2138/am-2015-5033

Fedele, F.G., Giaccio, B., Isaia, R. and Orsi, G. (2004). The Campanian Ignimbrite Eruption, Heinrich Event 4, and Palaeolithic Change in Europe: A High-Resolution Investigation. In Volcanism and the Earth's Atmosphere (eds A. Robock and C. Oppenheimer).

Fedele, L., Scarpati, C., Sparice, D., Perrotta, A., Laiena, F. (2016) A chemostratigraphic study of the Campanian Ignimbrite eruption (Campi Flegrei, Italy): Insights on magma chamber withdrawal and deposit accumulation as revealed by compositionally zoned stratigraphic and facies framework. Journal of Volcanology and Geothermal Research, 324, 105–117. doi:http://dx.doi.org/10.1016/j.jvolgeores.2016.05.019

Feisel Y., Castro J. M. and Dingwell D. B. (2019) Diffusion of F and Cl in dry rhyodacitic melt. American Mineralogist, 104, 1689–1699. 803.

Fisher, R. V., Orsi, G., Ort, M., Heiken, G. (1993) Mobility of a large-volume pyroclastic flow — emplacement of the Campanian ignimbrite, Italy. Journal of Volcanology and Geothermal Research, 56, 205–220. doi:10.1016/0377-0273(93)90017-L

Fortin, M.-A., Riddle, J., Desjardins-Langlais, Y., Baker,D.R. (2015) The effect of water on the sulfur concentration at sulfide saturation (SCSS) in natural melts, Geochimica et Cosmochimica Acta, Volume 160, Pages 100-116, https://doi.org/10.1016/j.gca.2015.03.022

Fourmentraux, C., Métrich, N., Bertagnini, A., Rosi, M., (2012) Crystal fractionation, magma step ascent, and syn-eruptive mingling: the Averno 2 eruption (Phlegraean Fields, Italy). Contribution to Mineralogy and Petrology, 163, 1121–1137. doi:10.1007/s00410-012-0720-1

Freymueller, J. T., Murray, J. B., Rymer, H., Locke, C. A. (2015). Chapter 64 - Ground Deformation, Gravity, and Magnetics, Editor(s): Haraldur Sigurdsson,The Encyclopedia of Volcanoes (Second Edition), Academic Press, Pages 1101-1123, https://doi.org/10.1016/B978-0-12-385938-9.00064-X.

Giaccio, B.,Hajdas, I., Isaia, R., Deino, A. (2017) High-precision 14C and 40Ar/39Ar dating of the Campanian Ignimbrite (Y-5) reconciles the time-scales of climatic-cultural processes at 40 ka. Scientific Reports. 7. 10.1038/srep45940.

Gonnermann, H.M., Foster, J.H., Poland, M., Wolfe, C.J., Brooks, B. a., Miklius, A. (2012) Coupling at Mauna Loa and Kīlauea by stress transfer in an asthenospheric melt layer. Nature Geoscience, 5, 826–829. doi:10.1038/ngeo1612

Gurioli L, Muro AD, Vlastélic I, Moune S, Thivet S, Valer M, Villeneuve N, Boudoire G, Peltier A, Bachèlery P, Ferrazzini V, Métrich N, Benbakkar M, Cluzel N, Constantin C, et al. Integrating field, textural, and geochemical monitoring to track eruption triggers and dynamics: a case study from Piton de la Fournaise *Solid Earth*. 9: 431-455. DOI: 10.5194/Se-9-431-2018 Huber, C., Townsend, M., Degruyter, W. *et al.* (2019) Optimal depth of subvolcanic magma chamber growth controlled by volatiles and crust rheology. Nature Geoscience, 12, 762–768. https://doi.org/10.1038/s41561-019-0415-6

Iacono Marziano, G., Schmidt, B.C., Dolfi, D. (2007) Equilibrium and disequilibrium degassing of a phonolitic melt (Vesuvius AD 79 “white pumice”) simulated by decompression experiments. Journal of Volcanology and Geothermal Reseach, 161, 151–164. doi:10.1016/j.jvolgeores.2006.12.001

Karakas, O., Degruyter, W., Bachmann, O. *et al.* (2017) Lifetime and size of shallow magma bodies controlled by crustal-scale magmatism. Nature Geoscience, 10, 446–450. https://doi.org/10.1038/ngeo2959

Le Bas, M.J., Le Maitre, R.W., Streckeisen, A., Zanettin, B. (1986) A chemical classification of volcanic rocks based on the total alkali silica diagram. Journal of Petrology, 27, 745–750. doi:10.1093/petrology/27.3.745

Lirer, L., Petrosino, P., Alberico, I. (2010) Hazard assessment at volcanic fields: The Campi Flegrei case history. Journal of Volcanology and Geothermal Reseach, 112, 53–73. doi:10.1016/S0377-0273(01)00234-7

Lowenstern, J.B. (1994) Chlorine, fluid immiscibility and degassing in peralkaline magmas from Pantelleria, Italy, American Mineralogist, 79, 353-369.

Magee, C. and others (2018). Magma Plumbing Systems: A Geophysical Perspective, Journal of Petrology, Volume 59, Issue 6, Pages 1217–1251, https://doi.org/10.1093/petrology/egy064Mangiacapra, A., Moretti, R., Rutherford, M., Civetta, L., Orsi, G., Papale, P. (2008) The deep magmatic system of the Campi Flegrei caldera (Italy). Geophysical Research Letter, 35, 6–11. doi:10.1029/2008GL035550

Marianelli, P., Sbrana, A., Proto, M. (2006) Magma chamber of the Campi Flegrei supervolcano at the time of eruption of the Campanian Ignimbrite. Geology, 34, 937–940. doi:10.1130/G22807A.1

Melluso, L., De Gennaro, R., Fedele, L., Franciosi, F., Morra, V. (2012) Evidence of crystallization in residual, Cl–F-rich, agpaitic, trachyphonolitic magmas and primitive Mg-rich basalt–trachyphonolite interaction in the lava domes of the Phlegrean Fields (Italy). Geological Magazine, 149 (3), pp. 532–550.

Moretti, R., Arienzo, I., Orsi, G., Civetta, L., D’Antonio, M. (2013) The deep plumbing system of Ischia: a physico-chemical window on the fluid-saturated and CO_2-sustained Neapolitan Volcanism (Southern Italy). Journal of Petrology, 54, 951–984. doi:10.1093/petrology/egt002

Moretti, R., Arienzo, I., Di Renzo, V., Orsi, G., Arzilli, F., Brun, F., D'Antonio, M., Mancini, L., Deloule, E. (2019) Volatile segregation and generation of highly vesiculated explosive magmas by volatile-melt fining processes: The case of the Campanian Ignimbrite eruption, Chemical Geology, Volume 503, Pages 1-14, https://doi.org/10.1016/j.chemgeo.2018.10.001

Mormone, A., Piochi, M., Bellatreccia, F., De Astis, G., Moretti, R., Della Ventura, G., Cavallo, A., Mangiacapra, A. (2011) A CO_2-rich magma source beneath the Phlegraean Volcanic District (Southern Italy): Evidence from a melt inclusion study, Chemical Geology, Volume 287, Issues 1–2, Pages 66-80, https://doi.org/10.1016/j.chemgeo.2011.05.019.

Orsi, G. (2022) Volcanic and Deformation History of the Campi Flegrei Volcanic Field, Italy. In: Orsi, G., D'Antonio, M., Civetta, L. (eds) Campi Flegrei. Active Volcanoes of the World. Springer, Berlin, Heidelberg. https://doi.org/10.1007/978-3-642-37060-1_1

Orsi, G., D'Antonio, M., Civetta, L. (Eds.), 2022. Campi Flegrei - A Restless Caldera in a Densely Populated Area. Introduction. Active Volcanoes of the World Book Series. Springer, Berlin, Heidelberg, pp. 1–410. DOI: 10.1007/978-3-642-37060-1.

Orsi, G., Civetta, L., D'Antonio, M., Di Girolamo, P., Piochi, M. (1995) Step-filling and development of a three-layer magma chamber: the Neapolitan Yellow Tuff case history. Journal of Volcanology and Geothermal Research, 67, 291–312. doi:10.1016/0377-0273(94)00119-2

Orsi, G., D'Antonio, M., Vita, S. De, Gallo, G. (1992) The Neapolitan Yellow Tuff, a large-magnitude trachytic phreatoplinian eruption: eruptive dynamics, magma withdrawal and caldera collapse. Journal of Volcanology and Geothermal Research, 53, 275–287. doi:10.1016/0377-0273(92)90086-S

Orsi, G., Di Vito, M.A., Selva, J., Marzocchi, W. (2009) Long-term forecast of eruption style and size at Campi Flegrei caldera (Italy). Earth and Planetary Science Letter, 287, 265–276. doi:10.1016/j.epsl.2009.08.013

Orsi, G., Gallo, G., Heiken, G., Wohletz, K., Yu, E., Bonani, G. (1992) A comprehensive study of pumice formation and dispersal: the Cretaio Tephra of Ischia (Italy). Journal of Volcanology and Geothermal Research, 53, 329–354. doi:10.1016/0377-0273(92)90090-Z

Orsi, G., Gallo, G., Zanchi, A. (1991) Simple-shearing block resurgence in caldera depressions. A model from Pantelleria and Ischia. Journal of Volcanology and Geothermal Research, Volume 47, Issues 1–2, Pages 1-11.

Orsi, G., De Vita, S., Di Vito, M. (1996a) The restless, resurgent Campi Flegrei nested caldera (Italy): constraints on its evolution and configuration. Journal of Volcanology and Geothermal Research, 74, 179–214. doi:10.1016/S0377-0273(96)00063-7

Orsi, G., Piochi, M., Campajola, L., D'Onofrio, A., Gialanella, L., Terrasi, F. (1996b) 14C geochronological constraints for the volcanic history of the island of Ischia (Italy) over the last 5000 years. Journal of Volcanology and Geothermal Research, 71, 249–257.

Pabst, S., Wörner, G., Civetta, L., Tesoro, R. (2008) Magma chamber evolution prior to the Campanian Ignimbrite and Neapolitan Yellow Tuff eruptions (Campi Flegrei, Italy). Bulletin of Volcanology, 70, 961–976. doi:10.1007/s00445-007-0180-z

Parmigiani, A., Degruyer, W., Leclaire, S., Huber, C. and Bachmann, O. (2017). The mecanics of shallow magma reservoir outgassing. Geochemistry Geophysics Geosystems, 18, 2887-2905.

Pappalardo, L., Civetta, L., De Vita, S., Di Vito, M., Orsi, G., Carandente, Fisher, R.V. (2002)Timing of magma extraction during the Campanian Ignimbrite eruption (Campi Flegrei Caldera). Journal of Volcanology and Geothermal Research, 114, 479–497. doi:10.1016/S0377-0273(01)00302-X

Pappalardo, L., and Mastrolorenzo, G. (2012) Rapid differentiation in a sill-like magma reservoir: a case study from the campi flegrei caldera. Scientific Report, 2, 712. doi:10.1038/srep00712

Piochi, M., Mastrolorenzo, G., Pappalardo, L. (2005) Magma ascent and eruptive processes from textural and compositional features of Monte Nuovo pyroclastic products, Campi Flegrei, Italy. Bulletin of Volcanology, 67, 663–678. doi:10.1007/s00445-005-0410-1Pontesilli, A., Del Bello, E., Scarlato, P., Mollo, S., Ellis, B., Andronico, D., Taddeucci, J., Nazzari, M. (2023). The efficacy of high frequency petrological investigation at open-conduit volcanoes: The case of May 11 2019 explosions at southwestern and northeastern craters of Stromboli, Lithos, Volumes 454–455,107255, https://doi.org/10.1016/j.lithos.2023.107255.

Popa, R.-G., Bachmann, O., Ellis, B.S., Degruyter, W., Tollan, P., Kyriakopoulos, K. (2019) A connection between magma chamber processes and eruptive styles revealed at Nisyros-Yali volcano (Greece), Journal of Volcanology and Geothermal Research, 387, 106666,https://doi.org/10.1016/j.jvolgeores.2019.106666.

Popa, R. G., Tollan, P., Bachmann, O., Schenker, V., Ellis, B., and Allaz, J. M. (2021a). Water exsolution in the magma chamber favors effusive eruptions: Application of Cl-F partitioning behavior at the Nisyros-Yali volcanic area. *Chem. Geol.* 570, 120170. doi:10.1016/j.chemgeo.2021.120170

Popa, R. G., Bachmann, O., Huber, C. (2021b). Explosive or effusive style of volcanic eruption determined by magma storage conditions. Nature Geoscience. 14. 781–786. 10.1038/s41561-021-00827-9.

Pritchard, M.E., and Gregg, P.M. (2016) Geophysical evidence for silicic crustal melt in the continents: where, what kind, and how much? Elements 12, 121 LP-127.

Putirka, K.D. (2008) Thermometers and barometers for volcanic systems. Review in Mineralogy and Geochemistry, 69, 61–120. doi:10.2138/rmg.2008.69.3

Re, G., Corsaro, R. A., D'Oriano, C., et al. (2021). Petrological monitoring of active volcanoes: A review of existing procedures to achieve best practices and operative protocols during eruptions, Journal of Volcanology and Geothermal Research,Volume 419, 107365, https://doi.org/10.1016/j.jvolgeores.2021.107365.

Rosi, M., Vezzoli, L., Castelmenzano, A., Grieco, G. (1999) Plinian pumice fall deposit of the Campanian Ignimbrite eruption (Phlegraean Fields, Italy). Journal of Volcanology and Geothermal Research, 91, 179–198. doi:10.1016/S0377-0273(99)00035-9

Samaniego, P., Le Pennec,J.-L., Robin, C. et al. (2011). Petrological analysis of the pre-eruptive magmatic process prior to the 2006 explosive eruptions at Tungurahua volcano (Ecuador), Journal of Volcanology and Geothermal Research,Volume 199, Issues 1–2, Pages 69-84, https://doi.org/10.1016/j.jvolgeores.2010.10.010.

Scaillet, B., Pichavant, M., Cioni, R. (2008) Upward migration of Vesuvius magma chamber over the past 20,000 years. Nature, 455, 216–219. doi:10.1038/nature07232

Signorelli, S., Carroll, M.R. (2000) Solubility and fluid-melt partitioning of Cl in hydrous phonolitic melts. Geochimica and Cosmochimica Acta, 64, 2851–2862. doi:10.1016/S0016-7037(00)00386-0

Signorelli, S., Carroll, M.R. (2002) Experimental study of Cl solubility in hydrous alkaline melts: Constraints on the theoretical maximum amount of Cl in trachytic and phonolitic melts. Contribution to Mineralogy and Petrology, 143, 209–218. doi:10.1007/s00410-001-0320-y

Signorelli, S., Vaggelli, G., Francalanci, L., Rosi, M. (1999) Origin of magmas feeding the Plinian phase of the Campanian Ignimbrite eruption, Phlegrean Fields (Italy): Constraints based on matrix-glass and glass-inclusion compositions. Journal of Volcanology and Geothermal Research, 91, 199–220. doi:10.1016/S0377-0273(99)00036-0

Signorelli, S., Vaggelli, G., Romano, C., Carroll, M. (2001) Volatile element zonation in Campanian Ignimbrite magmas (Phlegrean Fields, Italy): evidence from the study of glass inclusions and matrix glasses. Contribution to Mineralogy and Petrology, 140, 543–553. doi:10.1007/s004100000213

Smith, V.C., Isaia, R., Pearce, N.J.G. (2011) Tephrastratigraphy and glass compositions of post-15 kyr Campi Flegrei eruptions: implications for eruption history and chronostratigraphic markers. Quaternay Science Review, 30, 3638–3660. doi:10.1016/j.quascirev.2011.07.012

Tonarini, S., D’Antonio, M., Di Vito, M.A., Orsi, G., Carandente, A. (2009) Geochemical and B-Sr-Nd isotopic evidence for mingling and mixing processes in the magmatic system that fed the Astroni volcano (4.1-3.8 ka) within the Campi Flegrei caldera (southern Italy). Lithos 107, 135–151. doi:10.1016/j.lithos.2008.09.012

Wallace, P.J. (2005) Volatiles in subduction zone magmas: Concentrations and fluxes based on melt inclusion and volcanic gas data. Journal of Volcanology and Geothermal Research, 140, 217–240. doi:10.1016/j.jvolgeores.2004.07.023

Walter, T.R., Shirzaei, M., Manconi, A., Solaro, G., Pepe, A., Manzo, M., Sansosti, E. (2014) Possible coupling of Campi Flegrei and Vesuvius as revealed by InSAR time series, correlation analysis and time dependent modeling. Journal of Volcanology and Geothermal Research, 280, 104–110. doi:10.1016/j.jvolgeores.2014.05.006

Webster, J.D., Goldoff, B., Sintoni, M.F., Shimizu, N., De Vivo, B. (2014) C-O-H-Cl-S-F volatile solubilities, partitioning, and mixing in phonolitic-trachytic melts and aqueous-carbonic vapor saline liquid at 200 MPa. Journal of Petrology, 55, 2217–2248. doi:10.1093/petrology/egu055

Webster, J.D., Vetere, F., Botcharnikov, R.E., Goldoff, B., McBirney, A., Doherty, A.L. (2015) Experimental and modeled chlorine solubilities in aluminosilicate melts at 1 to

7000 bars and 700 to 1250 °C: Applications to magmas of Augustine Volcano, Alaska. American Mineralogist, 100, 522–535.

Zollo, A., Maercklin, N., Vassallo, M., Dello Iacono, D., Virieux, J., Gasparini, P. (2008) Seismic reflections reveal a massive melt layer feeding Campi Flegrei caldera. Geophysical. Research Letter, 35, L12306. doi:10.1029/2008GL034242

Figure captions

Figure 1: **Campi Flegrei – Eruptive History.** a) Schematic map of Italy. b) Location of the Neapolitan area: Campi Flegrei, Somma-Vesuvio volcanic complex, the islands of Ischia and Procida. Outcrop locations shown in grey for CI; brown for Solchiaro; yellow for NYT; green for PP; blue for A-MS; red for As6; orange for CT and purple for MN. c) Digital terrain model map of the Phlegraean Fields caldera. Major calderas areas (CI, NYT), the area of volcano-tectonic collapse (A-MS) and edifices (As6 and MN) are marked. Outcrop locations are shown for PP, A-MS, As6 and MN eruptions. d) Schematic chronogram of the studied eruptions. Arrows refer to explosive eruptions, and their length and color reflect the estimated VEI (Volcanic Explosivity Index from Mastrolorenzo and Pappalardo, 2006).

Figure 2: **Cl behavior and evidence of the buffering effect in silicate melt (melt inclusion and residual glass composition). Example of A-MS eruption** a) The H_2O-NaCl-silicate melt pseudo-system (redrawn at 1,000°C from Driesner and Heinrich, 2017). Blue domain: the silicate melt is in equilibrium with two fluids: a vapor phase (H_2O and/or CO_2 and/or S-rich) and a brine (Cl rich). Within this subsolvus domain, at a fixed temperature, the Cl concentration in silicate melt is buffered. Orange domain:

the silicate melt equilibrates with a single fluid phase (vapor or brine). b) Cl vs Na_2O (wt%) diagram. Solid dark line: the behavior of an incompatible non-volatile component from the most primitive composition considered for CF (Solchiaro eruption; Esposito et al., 2011; black ellipse). Red triangles: MI data from the A-MS eruption (Arienzo et al., 2010a), and blue squares: the residual glass contents of the A-MS eruption (this study). c) Pressure estimate from the identified Cl buffer value (2b) using the experimental Cl solubility for the A-MS melt composition, a trachytic melt compositionally close to samples from the Campanian Ignimbrite for which the Cl solubility law (red dots and mean red line) exists. Purple line: pressure estimate from Cl buffer value with the associated uncertainty in dotted blue lines (from mean Cl value).

Figure 3: **Alkali-silica diagram for residual glass** (Le Bas et al., 1986) a) Residual glass composition for Campi Flegrei and Ischia. The EPMA data are from individual pumice clasts covering the whole specific density distribution for each eruptive layer (Table 1 in Supplementary Material). Each residual glass point represents a mean of at least 6 measurements. b) The same as figure (a) with data of the Solchiaro eruption (Procida).

Figure 4: **Halogen contents of residual glass.** Compositions of individual pumice clasts belonging to the density mode for each eruptive layer. Each residual glass point represents a mean of at least 6 EPMA point measurements (see Tables in Supplementary Material). The MN eruption data are corrected for microlite content (30%; Piochi et al., 2005). a) F versus CaO (wt%) variation diagram. F behaves as an incompatible element and can be used as a differentiation index. The least evolved

composition of Solchiaro is excluded here for clarity as the mean CaO range is between 9 - 13.5 wt% for F contents between 1,500-2,000 ppm. b) Cl versus F (wt%) variation diagram.

Figure 5: Relationship between the Cl buffering effect and stratigraphy for the CI fallout deposit at Acquafidia. a) Stratigraphy of the CI fallout deposit. b) Variation diagram of Cl versus F (wt%) in glass. The 3 groups of eruptive units for the CI are identified by 3 shades of brown, from light brown for the first eruptive units (highest Cl buffer value) to dark brown (lowest Cl buffer value), corresponding to the stratigraphy of the fallout (5a).

Figure 6: Sulfur (ppm) versus CaO (wt%) variation diagrams. Matrix glass (squares) and Melt Inclusions (diamonds, when analyzed) are shown for CI, NYT, PP, As-6, MN and CT eruptions. Color scheme as in figure 3. The minimum S detection limit with EPMA is 80 ppm. Symbols represent single point measurements. The uncertainty is within the symbol size for CaO and 5% for S. Data are given in Supplementary Material Table 2.

Figure 7: Cl buffering value and pressure estimates using the Cl experimental solubility law. For each eruption, the selected Cl experimental solubility law has been redrawn and the pressure domain is given (solid line: Cl buffer value representing pressure; dashed lines: uncertainty on pressure estimates based on uncertainty on Cl buffer value). a) CI eruption with its own Cl experimental solubility curves (trachytic composition). b) For NYT, PP and As-6 eruptions, as the composition straddles the trachyte and phonolite fields the pressure domain can be bracketed by the respective

solubility laws. c) A-MS and CT eruptions: the two available Cl experimental solubility curves for these trachytic composition are shown (red: CI composition and green: Pomici di Base eruption (Somma-Vesuvio volcanic complex) from (Signorelli and Carroll, 2002). Blue: A-MS eruption, and orange: CT eruption pressure estimate. d) MN eruption: Cl experimental solubility curves for a K-phonolite of similar composition (AD 79 eruption of Somma-Vesuvio volcanic complex from Signorelli and Carroll, 2000).

Figure 8: Cl buffering value and pressure estimates deduced from the Cl solubility model (Webster et al., 2015**).** Solid symbols: blue circle: modelled residual glass with no S correction; yellow circles, modelled residual glass with S correction of 30-40%. a) As6 eruption: measured Cl experimental and modelled Cl solubility at 90 MPa. Red diamonds: measured residual glass. b) PP eruption: measured Cl experimental and modelled Cl solubility at 100 MPa. Green diamonds: measured residual glass.

Figure 9: Pre-eruptive conditions: H_2O content estimates from Cl buffer values. Experimental H_2O solubility laws for trachytic (green curve; Di Matteo et al., 2004) and K-phonolite melts (orange curve; Iacono Marziano et al., 2007). Marks correspond to each determined pressure domain.

Figure 10: Architecture of the shallow magma plumbing systems of Campi Flegrei and Ischia. Vertical axis: Pressure is converted into depth using a lithostatic pressure gradient of 25 MPa/km. Rectangular box: pressure domain obtained using the Cl experimental solubility law. Star: pressure obtained by the Cl solubility model. Averno

2 eruption: data from Fourmentraux et al. (2012). For AM-S: the blue arrow indicates the possible deepening of the reservoir due to CO_2 fluxing (see text for discussion).

Supplementary Material

SM 1 – Outcrop locations

SM 2 – Material and Methods

SM 3 – Textural characteristics

Tables in Supplementary Material

Table 1: Residual glass composition; major and volatile elements. Data of glass compositions are recalculated to 100% on anhydrous basis. Each point represents a mean value (with Standard Deviation (SD%) indicated). n: number of point analyses.

Table 2: (a) Melt Inclusion (MI) composition (major and volatile (F, Cl, S) elements). FeS analyses represent the globules of sulfur analyzed in CT and NYT eruptions. **(b) Residual glass (RG) composition; major and volatile (F, Cl, S) elements.** Data of glass composition (MI and RG) are recalculated to 100% on anhydrous basis. BDL: Below Detection Limit. Each value is for a single point on one sample of the selected eruptive unit. The detection limit for S is 80 ppm. The uncertainty is below 5% for F, Cl and S measurements by electronic microprobe (EPMA, Camparis, France; See Supplementary Material SM2).

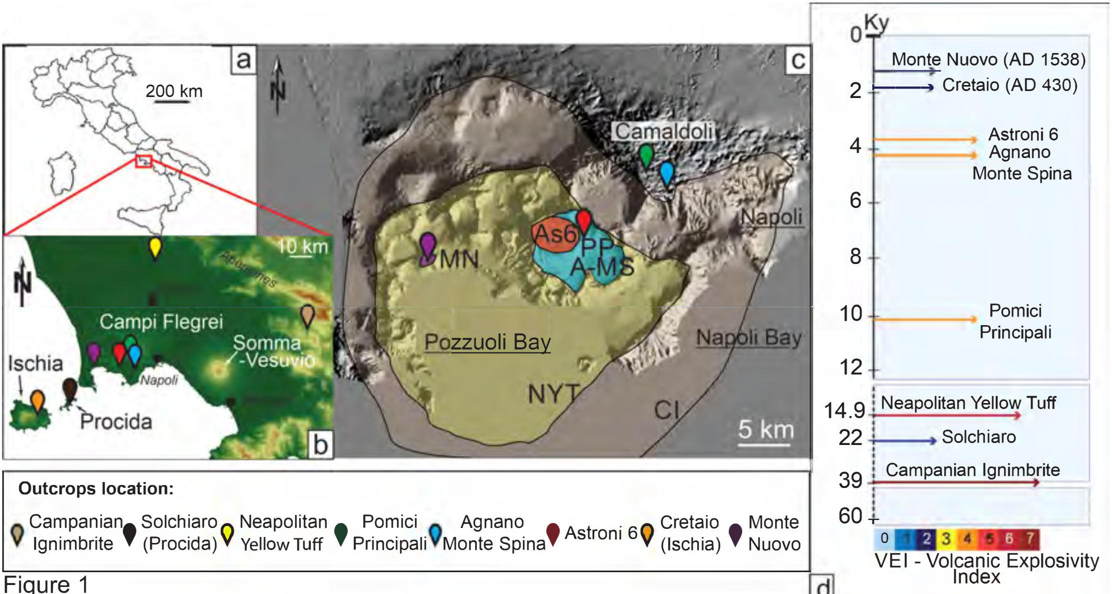
a
200 km
b
10 km
Apennines
Campi Flegrei
Somma
-Vesuvio
Ischia
Napoli
Procida
c
Camaldoli
Napoli
As6
PP
A-MS
MN
Pozzuoli Bay
Napoli Bay
NYT
CI
5 km
Outcrops location:
Campanian Ignimbrite
Solchiaro (Procida)
Neapolitan Yellow Tuff
Pomici Principali
Agnano Monte Spina
Astroni 6
Cretaio (Ischia)
Monte Nuovo
Ky
0
2
4
6
8
10
12
14.9
22
39
60
Monte Nuovo (AD 1538)
Cretaio (AD 430)
Astroni 6
Agnano
Monte Spina
Pomici
Principali
Neapolitan Yellow Tuff
Solchiaro
Campanian Ignimbrite
0 1 2 3 4 5 6 7
VEI - Volcanic Explosivity Index
d

Figure 1

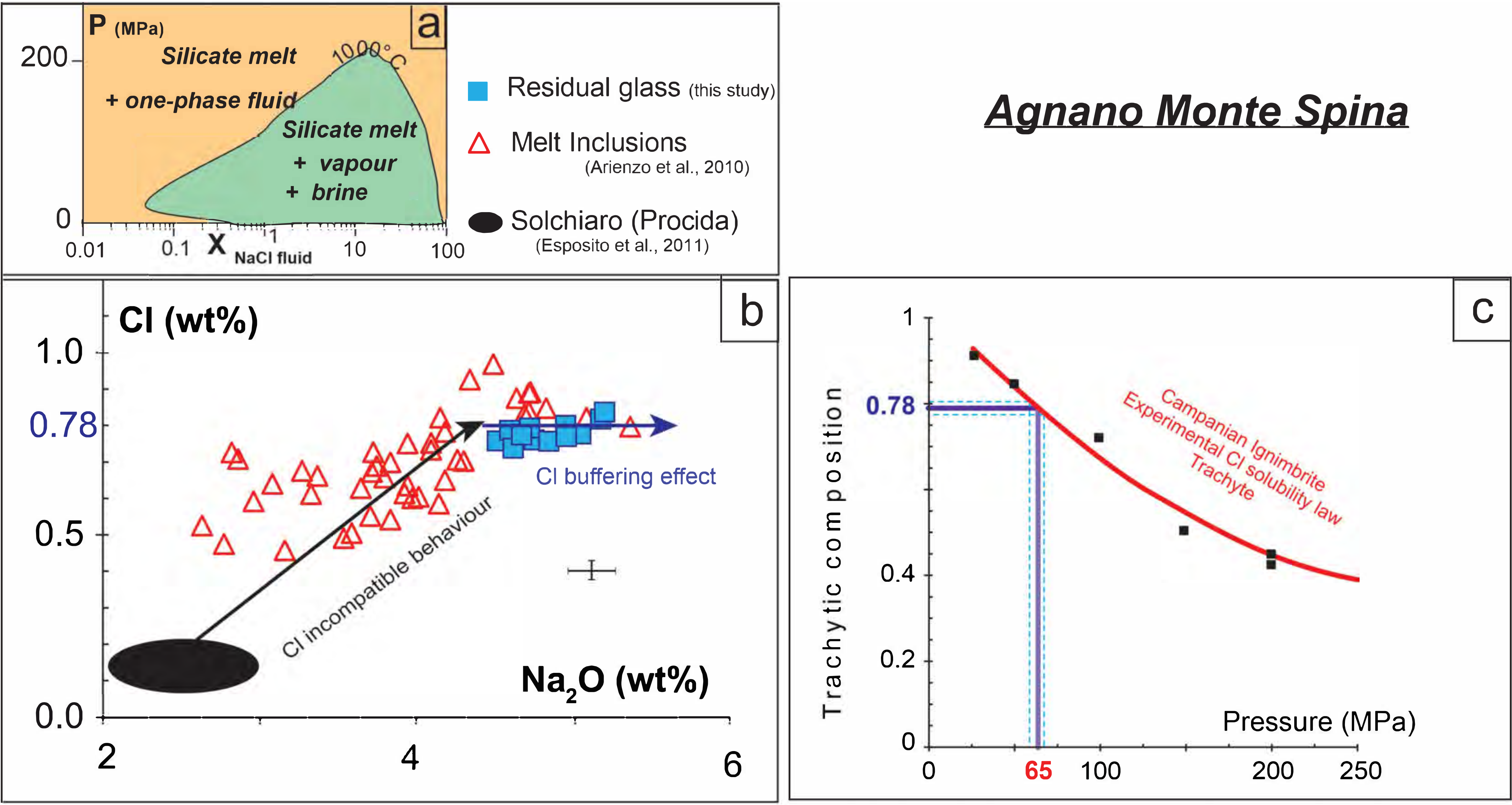

P (MPa)
a
200
0
Silicate melt
+ one-phase fluid
1000°C
Silicate melt
+ vapour
+ brine
0.01
0.1
X NaCl fluid
1
10
100
Residual glass (this study)
Melt Inclusions
(Arienzo et al., 2010)
Solchiaro (Procida)
(Esposito et al., 2011)
Agnano Monte Spina
b
Cl (wt%)
1.0
0.78
0.5
0.0
Cl buffering effect
Cl incompatible behaviour
Na2O (wt%)
2
4
6
c
1
0.78
0.4
0.2
0
Trachytic composition
Campanian Ignimbrite
Experimental Cl solubility law
Trachyte
Pressure (MPa)
0
65
100
200
250

Figure 2

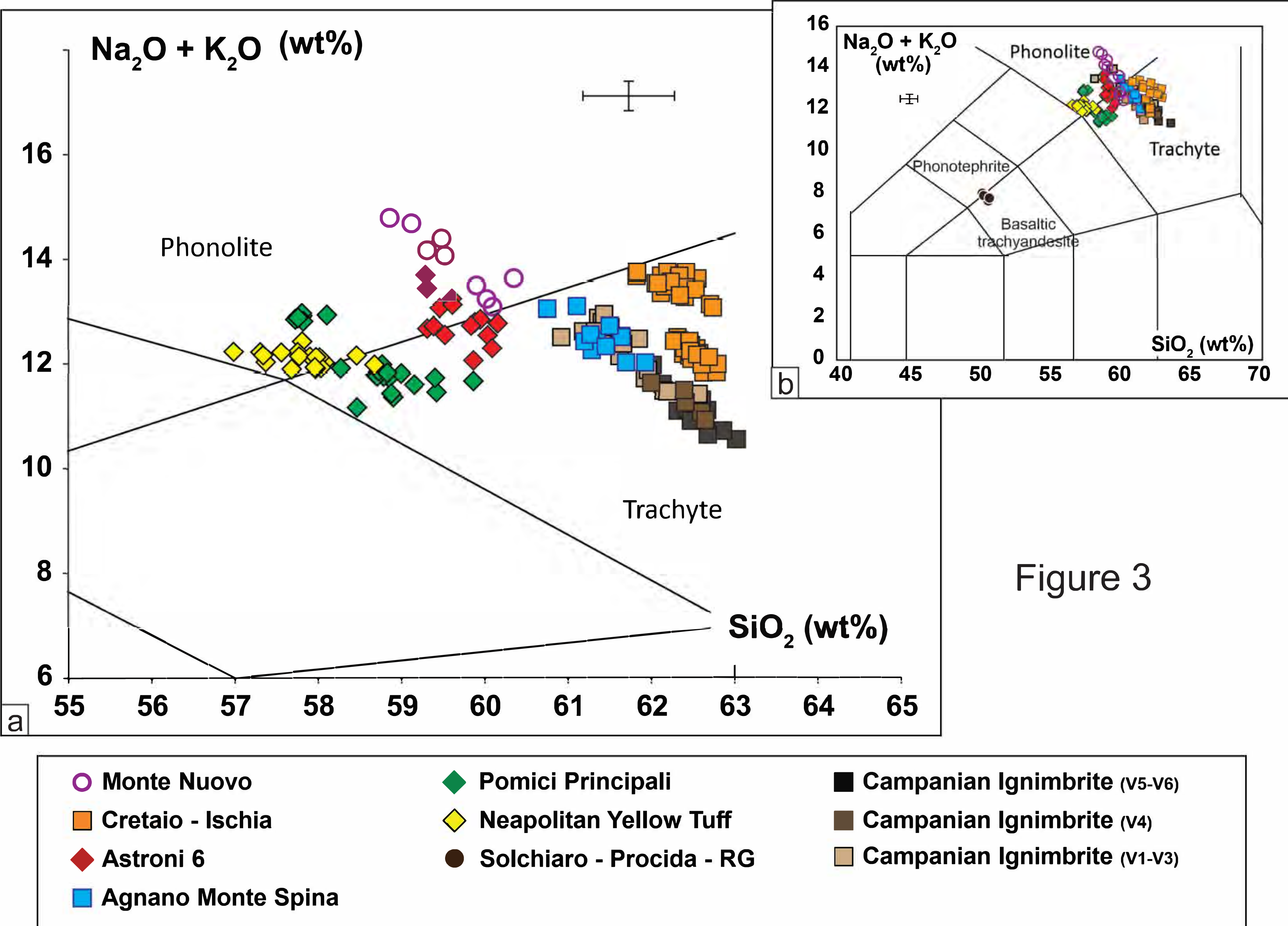

Na2O + K2O (wt%)
Phonolite
Trachyte
SiO2 (wt%)
a
b
Phonotephrite
Basaltic trachyandesite
16
14
12
10
8
6
4
2
0
55
56
57
58
59
60
61
62
63
64
65
40
45
50
70
Monte Nuovo
Cretaio - Ischia
Astroni 6
Agnano Monte Spina
Pomici Principali
Neapolitan Yellow Tuff
Solchiaro - Procida - RG
Campanian Ignimbrite (V5-V6)
Campanian Ignimbrite (V4)
Campanian Ignimbrite (V1-V3)

Figure 3

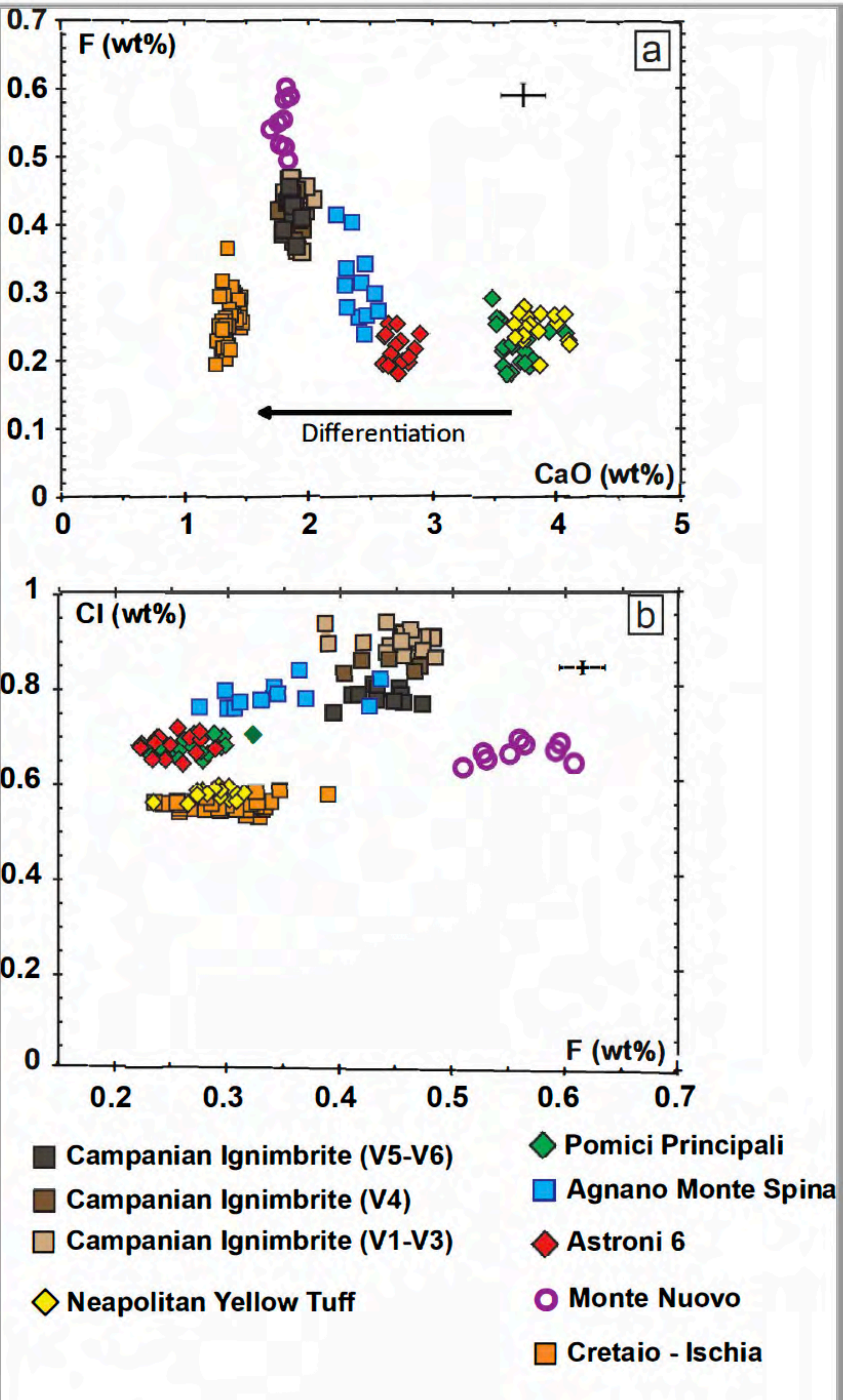

F (wt%)
a
Differentiation
CaO (wt%)
0.7
0.6
0.5
0.4
0.3
0.2
0.1
0
0
1
2
3
4
5
Cl (wt%)
b
F (wt%)
1
0.8
0.6
0.4
0.2
0
0.2
0.3
0.4
0.5
0.6
0.7
Campanian Ignimbrite (V5-V6)
Campanian Ignimbrite (V4)
Campanian Ignimbrite (V1-V3)
Neapolitan Yellow Tuff
Pomici Principali
Agnano Monte Spina
Astroni 6
Monte Nuovo
Cretaio - Ischia

Figure 4

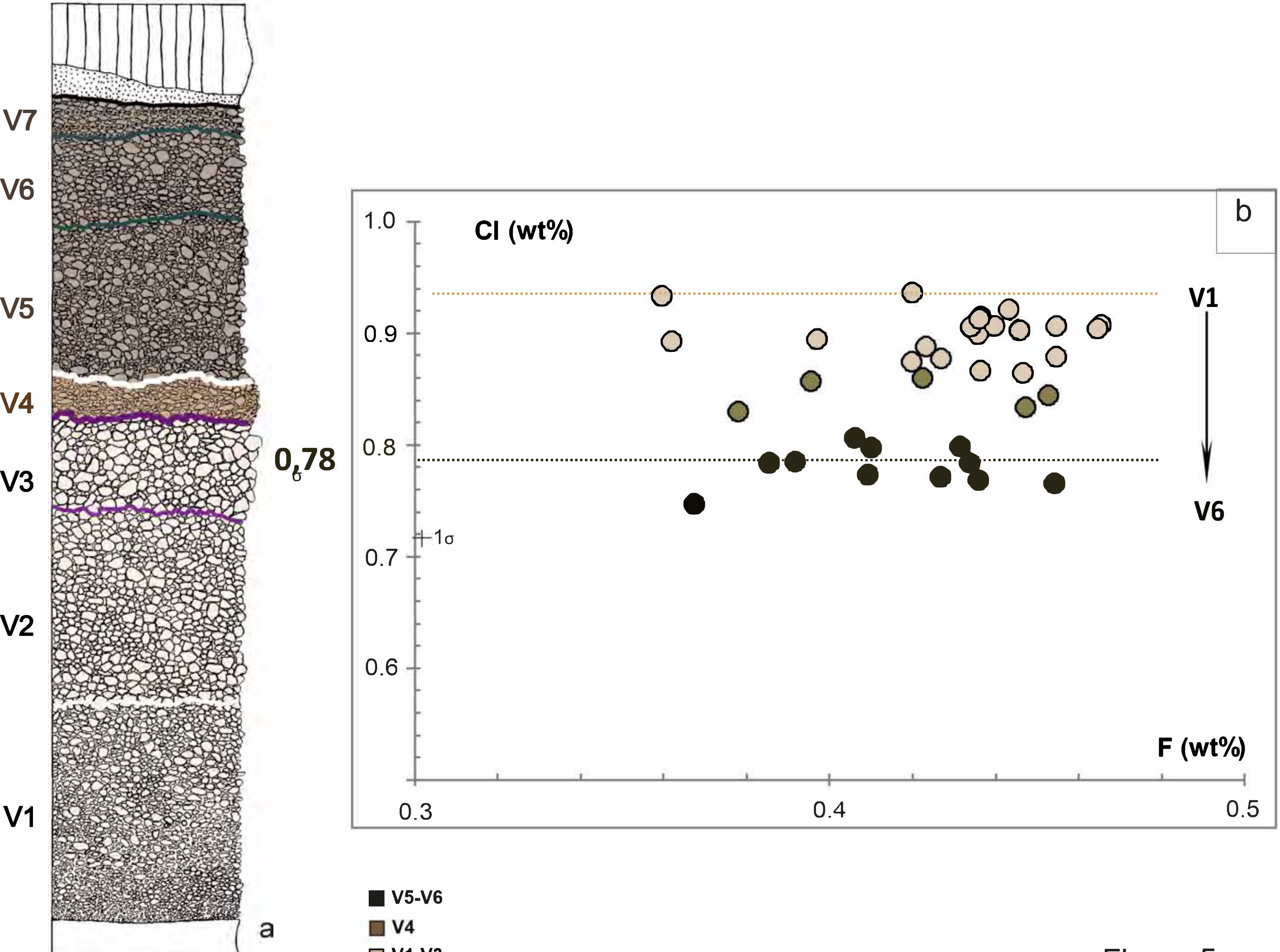
V7
V6
V5
V4
V3
V2
V1
0,78
a
b
Cl (wt%)
1.0
0.9
0.8
0.7
0.6
1σ
V1
V6
F (wt%)
0.3
0.4
0.5
V5-V6
V4
V1-V3

Figure 5

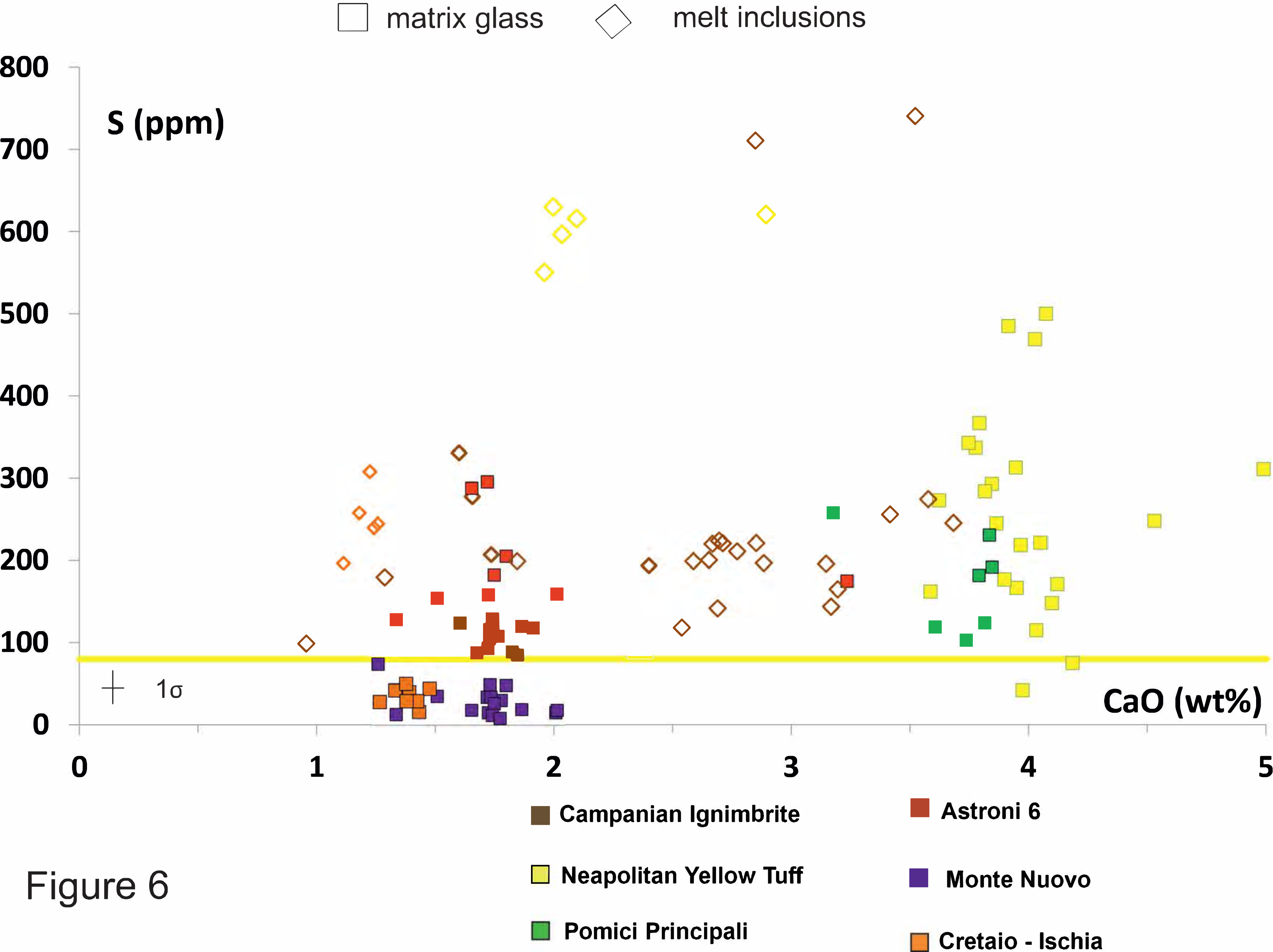

matrix glass
melt inclusions
S (ppm)
CaO (wt%)
1σ
0
100
200
300
400
500
600
700
800
0
1
2
3
4
5
Campanian Ignimbrite
Astroni 6
Neapolitan Yellow Tuff
Monte Nuovo
Pomici Principali
Cretaio - Ischia

Figure 6

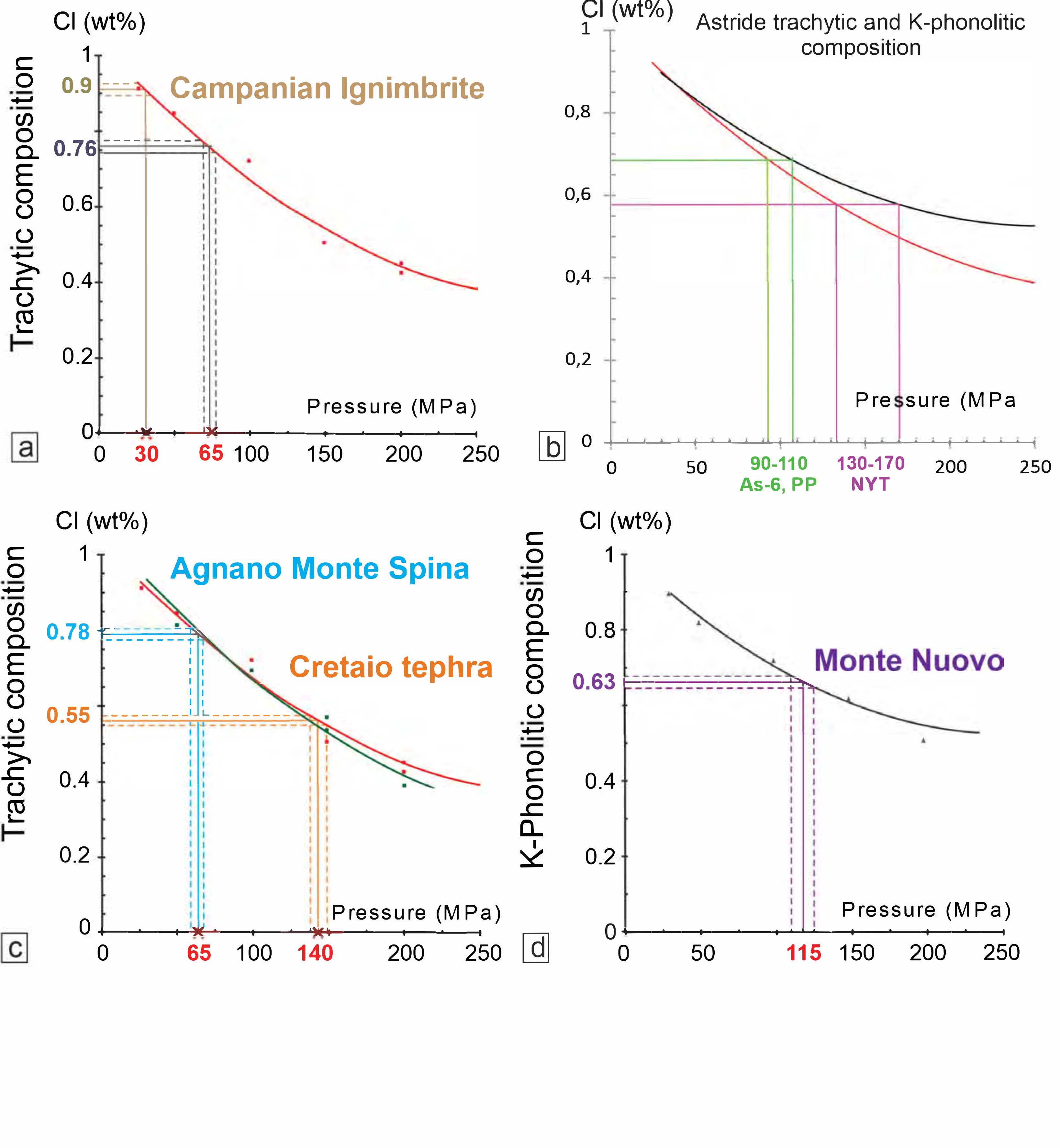

Cl (wt%)
Trachytic composition
Campanian Ignimbrite
0.9
0.76
Pressure (MPa)
30
65
a
Cl (wt%)
Astride trachytic and K-phonolitic composition
Pressure (MPa
90-110
As-6, PP
130-170
NYT
b
Cl (wt%)
Trachytic composition
Agnano Monte Spina
0.78
Cretaio tephra
0.55
Pressure (MPa)
65
140
c
Cl (wt%)
K-Phonolitic composition
Monte Nuovo
0.63
Pressure (MPa)
115
d

Figure 7

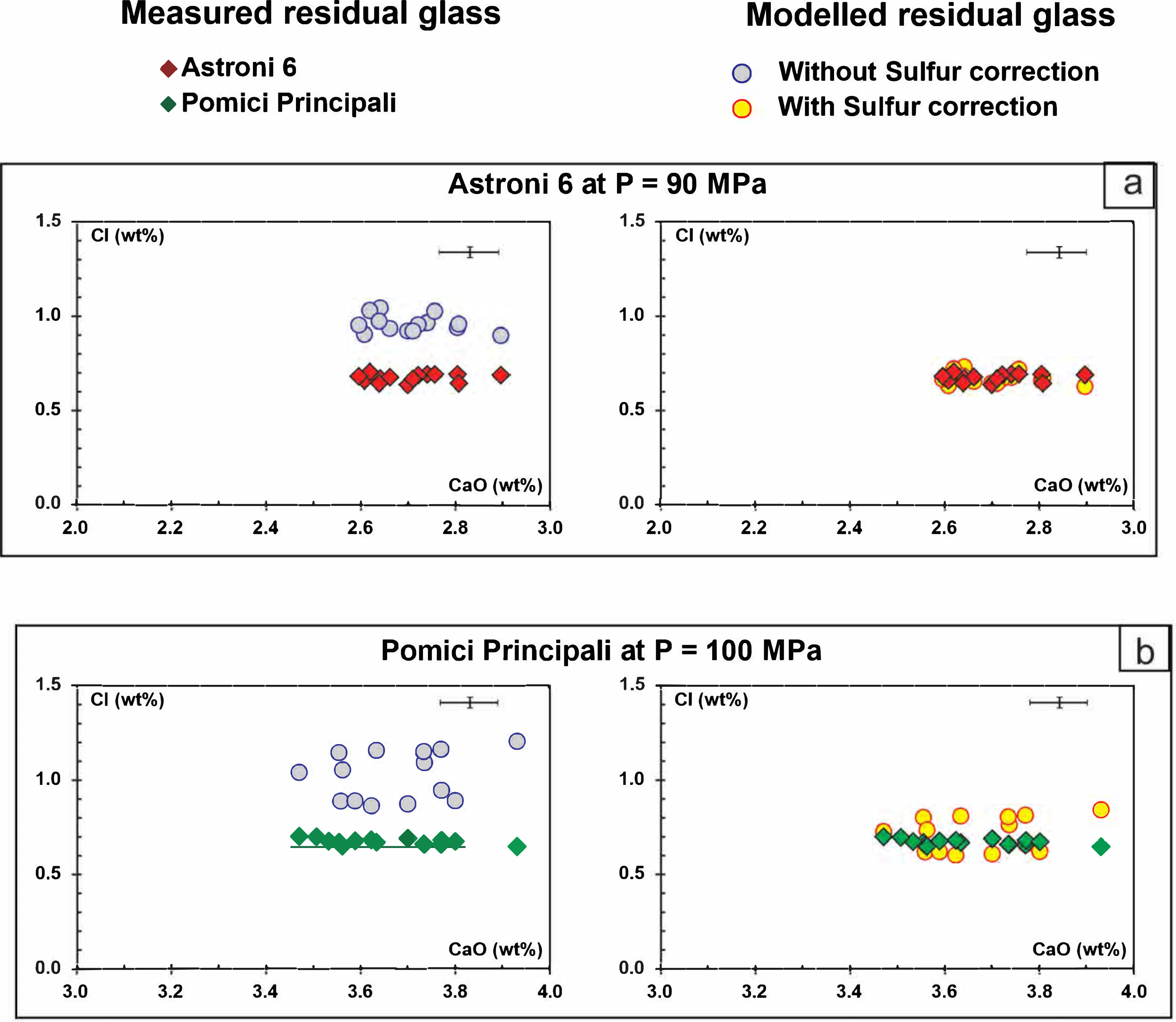
Measured residual glass
Astroni 6
Pomici Principali
Modelled residual glass
Without Sulfur correction
With Sulfur correction
Astroni 6 at P = 90 MPa
a
Cl (wt%)
CaO (wt%)
1.5
1.0
0.5
0.0
2.0
2.2
2.4
2.6
2.8
3.0
Pomici Principali at P = 100 MPa
b
3.0
3.2
3.4
3.6
3.8
4.0

Figure 8

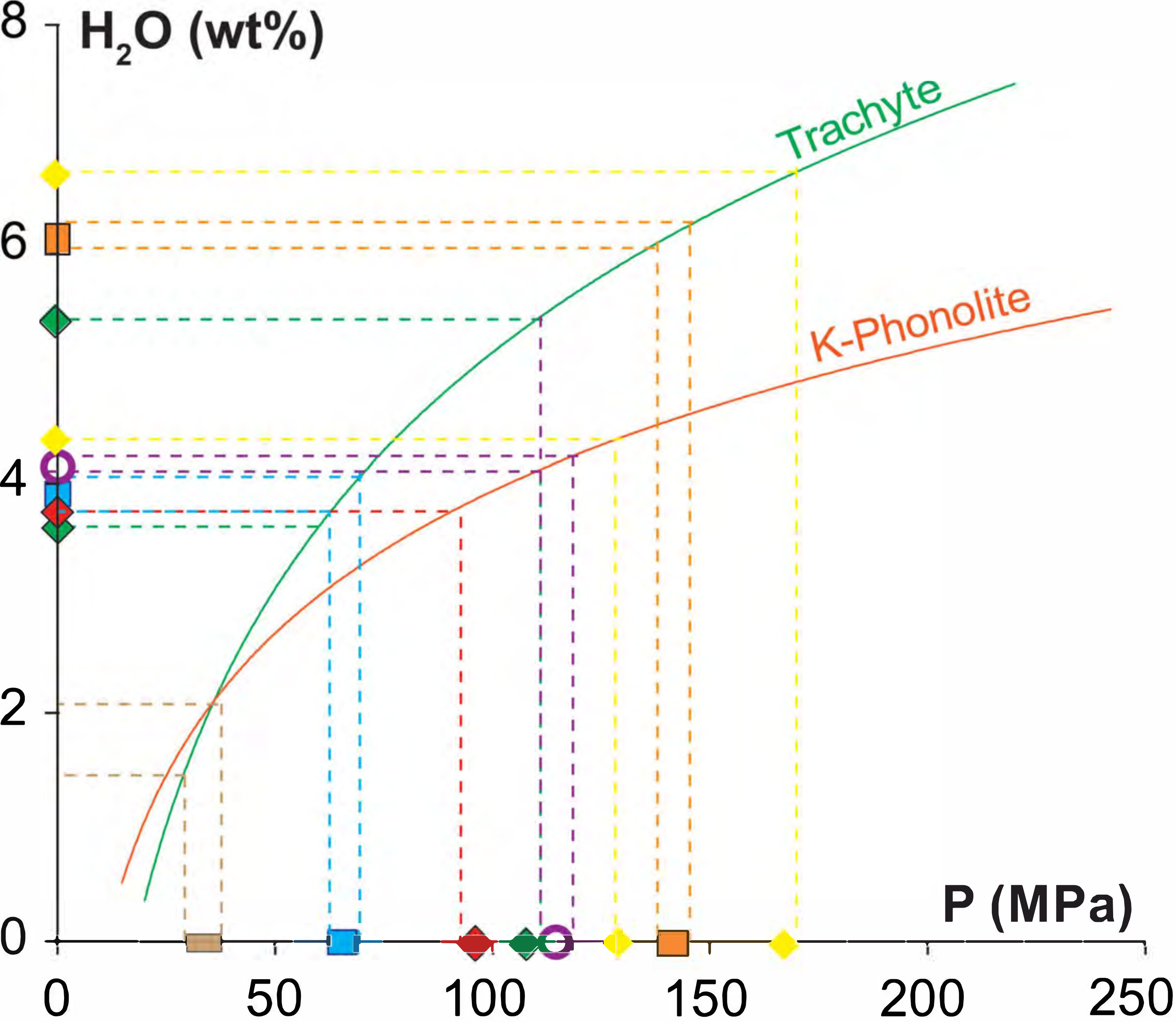

	Pre-eruptive H_2O content (wt%)
MN	4 - 4.2
CT	6 - 6.2
As6	3.8 - 5.5
PP	
A-MS	3.8 - 4.1
NYT	4.2 - 6.5
CI	1.5 - 2

Figure 9

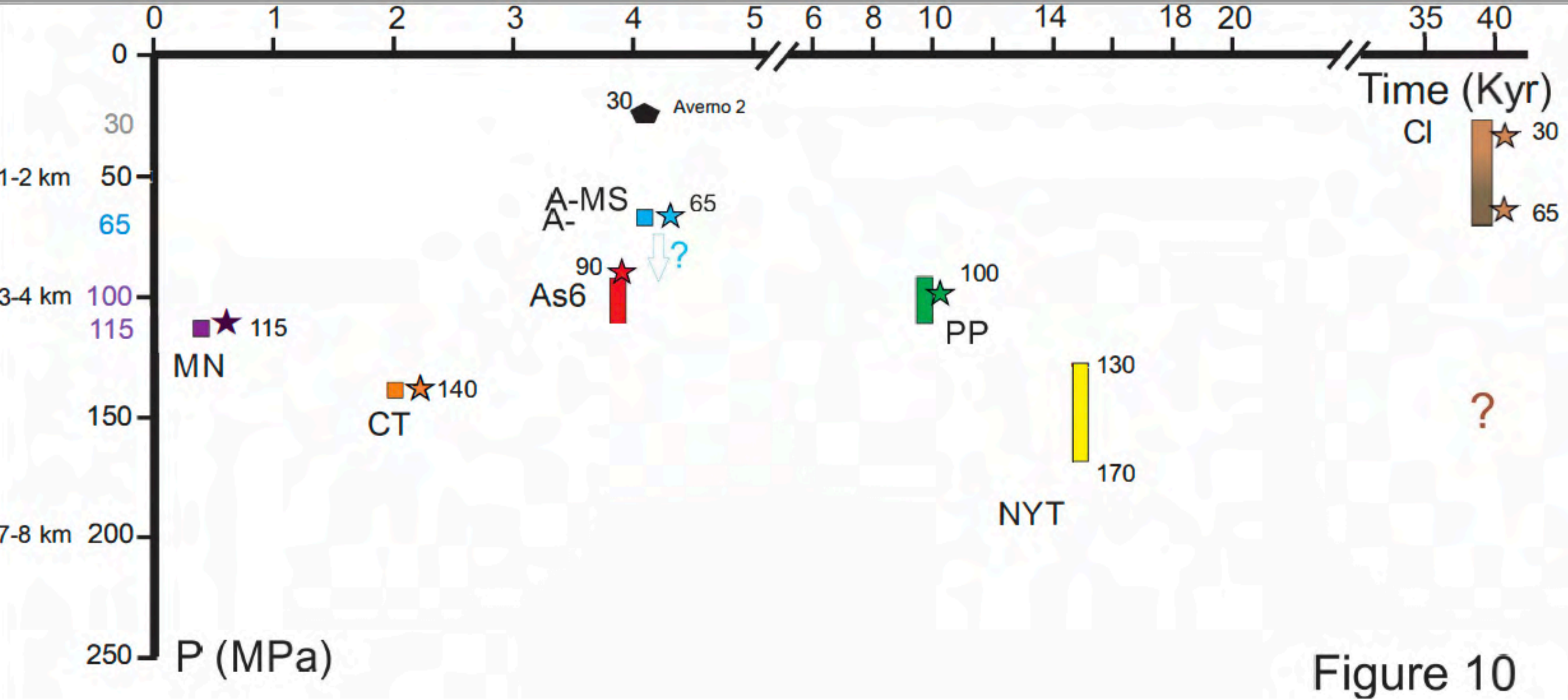

Time (Kyr)
0
1
2
3
4
5
6
8
10
14
18
20
35
40
0
30
1-2 km
50
65
3-4 km
100
115
150
7-8 km
200
250
P (MPa)
30
Averno 2
A-MS
A-
65
?
90
As6
115
MN
140
CT
100
PP
130
170
NYT
CI
30
65
?

Figure 10